Journal of Engineering Physics and Thermophysics, Vol. 83, No. 6, 2010

DEFLAGRATION-TO-DETONATION TRANSITION IN GASES IN TUBES WITH CAVITIES

N. N. Smirnov, V. F. Nikitin, and Yu. G. Phylippov

UDC 634.222.2 + 662.7

The existence of a supersonic second combustion mode — detonation — discovered by Mallard and Le Chatelier and by Berthélot and Vieille in 1881 posed the question of mechanisms for transition from one mode to the other. In the period 1959–1969, experiments by Salamandra, Soloukhin, Oppenheim, and their coworkers provided insights into this complex phenomenon. Since then, among all the phenomena related to combustion processes, deflagration-to-detonation transition is, undoubtedly, the most intriguing one. Deflagration-to-detonation transition (DDT) in gases is connected with gas and vapor explosion safety issues. Knowing mechanisms of detonation onset control is of major importance for creating effective mitigation measures addressing two major goals: to prevent DDT in the case of mixture ignition, or to arrest the detonation wave in the case where it has been initiated. A new impetus to the increase in interest in deflagration-to-detonation transition processes was given by the recent development of pulse detonation devices.

The probable application of these principles to creation of a new generation of engines put the problem of effectiveness of pulse detonating devices at the top of current research needs. The effectiveness of the pulse detonation cycle turned out to be the key factor characterizing the Pulse Detonation Engine (PDE), whose operation modes were shown to be closely related to periodical onset and degeneration of a detonation wave. Those unsteady-state regimes should be self-sustained to guarantee a reliable operation of devices using the detonation mode of burning fuels as a constitutive part of their working cycle. Thus deflagration-to-detonation transition processes are of major importance for the issue. Minimizing the predetonation length and ensuring stability of the onset of detonation enable one to increase the effectiveness of a PDE. The DDT turned out to be the key factor characterizing the PDE operating cycle. Thus, the problem of DDT control in gaseous fuel–air mixtures became very acute.

This paper contains results of theoretical and experimental investigations of DDT processes in combustible gaseous mixtures. In particular, the paper investigates the effect of cavities incorporated in detonation tubes at the onset of detonation in gases. Extensive numerical modeling and simulations allowed studying the features of deflagration-to-detonation transition in gases in tubes incorporating cavities of a wider cross section. The presence of cavities substantially affects the combustion modes being established in the device and their dependence on the governing parameters of the problem. The influence of geometrical characteristics of the confinement and flow turbulization on the onset of detonation and the influence of temperature and fuel concentration in the unburned mixture are discussed. It was demonstrated both experimentally and theoretically that the presence of cavities of wider cross section in the ignition part of the tube promotes DDT and shortens the predetonation length. At the same time, cavities incorporated along the whole length or in the far-end section inhibit detonation and bring about the onset of low-velocity galloping detonation or galloping combustion modes. The presence of cavities in the ignition section turns an increase in the initial mixture temperature into a DDT-promoting factor instead of a DDT-inhibiting factor.

Keywords: *deflagration, detonation, shock waves, combustion, flame, transition, onset.*

Introduction. In 1881, Mallard and Le Chatelier [1] and Berthélot and Vieille [2] were the first to face the deflagration-to-detonation transition process. On investigating flame propagation in homogeneous gaseous mixtures, they unexpectedly detected the onset of a supersonic mode of combustion wave traveling at velocities of thousands of

Faculty of Mechanics and Mathematics, Moscow M. V. Lomonosov State University, Moscow, 119992, Russia; e-mail: ebifsun1@mech.math.msu.su. Publisher in Inzhenerno-Fizicheskii Zhurnal, Vol. 83, No. 6, pp. 1212–1238, November–December, 2010. Original article submitted May 19, 2010.

1062-0125/10/8306-1287©2010 Springer Science+Business Media, Inc.

meters per second. This combustion mode was called "false" or "out of tone" combustion, which in French sounds like "détonation," being originated from the French verb "détonner." The existence of two alternative velocities for the combustion process needed a theoretical explanation, which was given in 1893 by Associate Professor of Moscow University V. A. Mikhelson in his paper "On normal combustion velocity of explosive gaseous mixtures" [3]. Based on the already published papers of Rankine [4] and Hugoniot [5], Mikhelson's was the first to explain that the mechanism of flame propagation in detonation was not the heat conductivity, but "adiabatic heating up to the ignition point in shock waves." That was the birth of the classical theory of detonation, which found its further development in the papers of Chapman [6] and Jouguet [7].

On analyzing the initiation of detonation by a local energy release in gases, one could distinguish three scenarios. The first scenario: the energy release brings about the formation of a shock wave strong enough to activate chemical reactions in the compressed gas due to temperature increase. Energy release behind the shock, due to activated chemistry supports the leading shock, preventing its attenuation and keeping its velocity at the level by Chapmen–Jouguet detonation. Thus, the velocity of the wave propagation becomes independent of the initiation conditions. This scenario was investigated with great completeness in [8–10] and successive studies by Chernyi, Levin, Markov and coworkers.

The second scenario of detonation initiation takes place under the condition where the intensity of the shock wave formed due to initial energy release is too small and its attenuation is too fast to initiate substantial energy release in the shock-compressed gas, but heating of the gas in the zone of energy release is sufficient to initiate chemical reactions. Then a normal combustion wave propagates from the zone of initial energy release. The propagation mechanism of this wave (the mechanism of reaction activation in the neighboring layers of the gas) is different from the shock wave compression that is due to heat conduction to those layers from the burnt gas. The propagating combustion wave brings about acceleration and turbulization of gas flow ahead of its front, which, in turn, leads to acceleration of the turbulent flame. Compression waves ahead of the flame front converge into one or several shock waves overtaking each other. The flame-propagation velocity could either stabilize on reaching some value, thus forming the structure of a turbulent flame preceded by a shock wave moving with a higher velocity and leaving behind the flame zone, or flame acceleration could bring about the onset of detonation, thus changing the combustion-wave propagation mechanism. The last process was called the deflagration-to-detonation transition. The present paper is focused on studying these types of processes.

There could be intermediate scenarios of detonation initiation as a combination of the two limiting cases: creating an initial ignition zone and a low-intensity shock, which is not strong enough to initiate chemical reactions but is sufficient to facilitate DDT. Such scenarios could be observed in flame jet ignition [11].

Investigations of deflagration-to-detonation transition in hydrogen–oxygen mixtures [12–16, 76, 77] and later in hydrocarbon–air mixtures [17–19] showed the multiplicity of the transition-process scenarios. The various modes of detonation onset were shown to depend on the particular flow pattern created by the accelerating flame, thus making the transition process irreproducible in its detailed sequence of events. At present, there exist different points of view on the DDT mechanism: the "explosion in explosion" mechanism by Oppenheim [14, 16] and the gradient mechanism of "spontaneous flame" by Zeldovich [20].

Later theoretical analysis showed that microscale nonuniformities (temperature and concentration gradients) arising in local exothermic centers ("hot spots") ahead of the flame zone could be sufficient for the onset of detonation or normal deflagration [21–27]. Analysis and comparison of theoretical and experimental results showed that self-ignition in one or in a number of hot spots ahead of the accelerating flame followed by the onset of either detonation or deflagration waves brings about a multiplicity of transition scenarios [28, 29]. Shock waves ahead of the flame could occur due to initiating energy release and due to the piston effect of the expanding flame. Reflection of these compression waves from the walls of the vessels and the contact surface between burnt and unburned gases brings about recirculation of waves, their amplitude growing due to wave–flame interaction [30, 31]. The common feature of all those scenarios is the formation of local exothermic centers according to the stochastic Oppenheim mechanism followed by the onset of detonation at a microscale in one of the exothermic centers according to the spontaneous Zeldovich mechanism [28]. The first numerical DDT investigations carried out using the 1-D Navier–Stokes model [70] as well as subsequent analysis [71] also demonstrated this effect. Other investigators explain the detonation-wave onset not by spontaneous flame acceleration within a single exothermic center but rather by restructuring of the flow, being

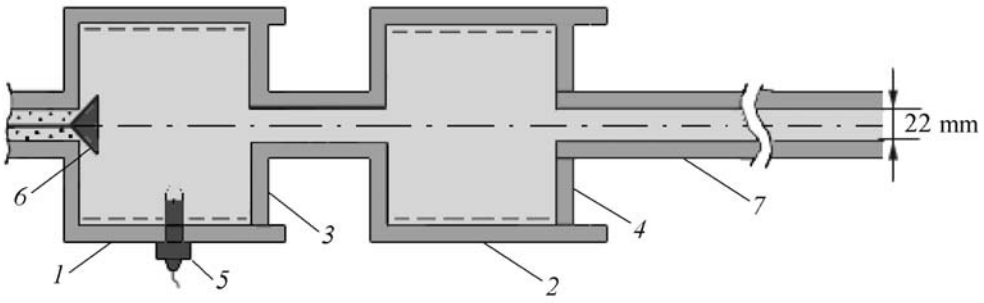

Fig. 1. Apparatus for DDT investigations with variable volume cavities.

the result of flame interaction with the zone of elevated temperature ahead, which leads in the long run to the formation of ignition delay gradients sufficient for spontaneous detonation onset [61, 62]. There is currently no experimental evidence that DDT could take place in an open space without any obstacles and wave reflections, nor has anyone obtained such a DDT in numerical simulations.

A third mechanism of initiation, which looks like an intermediate one, can be distinguished. In the first stage, mixture ignition following the second scenario takes place, which gives birth to slow flame propagation in a weak combustion mode, which does not initiate a strong enough shock wave ahead of flame zone. Then the combustion zone is affected by a strong shock wave formed elsewhere [32, 33, 63]. The intensity of that secondary shock wave is usually less than that necessary for direct detonation initiation in a cold unreacted mixture, but it is sufficient for detonation initiation in interaction with heated layers in the vicinity of the flame zone. Experimental and theoretical investigations [32, 33] of the reflected shock–laminar flame interactions bringing about the onset of detonation also showed that the transition to detonation in a hot spot takes place through the gradient mechanism, while the shock and flame interactions were important for creating the proper conditions for the hot spots to occur.

To promote DDT in tubes, effective measures were suggested: introducing the Shchelkin spiral in the ignition section [34]; incorporating wider cavities in the ignition section [17, 28]; blocking the initial part of the tube with orifice plates [35]. To bring detonation to decay, detonation arrestors are used [36]. Wider cavities were discovered to provide for DDT both a promoting effect and an inhibiting effect depending on their number and location [37]. Combustion-wave propagation in tubes incorporating cavities was investigated in [37–39, 56, 57]. Kinetics of chemical reactions plays an essential role in deflagration-to-detonation transition as well. It was first demonstrated in [40] that, contrary to existing opinion, ignition of hydrogen–air mixtures at atmospheric pressure near the third limit follows the chain branching mechanism. The competition of chain branching and termination along with self-heating determines the kinetics of the process. Introducing small amounts of additives causing chain termination could substantially inhibit DDT.

Experiments on formation of detonation waves in a stream of fuel components demonstrated different features of ignition being a function of initiation energy [64–67]. Rapid flame acceleration was detected in the stream of mixing components (v = 50–150 m/s), and successive formation of detonation exceeding the Chapman–Jouguet parameters at a distance of 8–12 diameters, with initiation energy not exceeding 20% of the energy for direct initiation.

Theoretical and experimental investigations of DDT were successfully used for evaluating pulse detonation engines and developing prototypes [54, 56–60, 69]. In particular, "Smirnov's cavities" were reported to have been effective for developing a research pulse detonation engine [69].

The present investigation was aimed at revealing the effects of wider cavities, mixture composition, and temperature in DDT and its control.

Experimental Investigations. Experimental investigations of the initiation of pulsed detonation regimes in gaseous mixtures of hydrocarbon fuels with air were undertaken. A detailed description of the experimental procedure and apparatus can be found in [28]. Physical experiments were undertaken using a confinement incorporating two wider cavities in the ignition section of the detonation tube, as shown in Fig. 1.

Investigation of the influence of confinement geometry on turbulent flame acceleration and detonation onset or degeneration was performed using cylindrical cavities (cavities) of variable volume in experiments. The side walls of the cavities *1* and *2* (Fig. 1), having a thread on the inner surface, made it possible to screw the cylindrical plates *3* and *4* more or less deeply into the cavities, thus varying the volume. The mixture was ignited in cavity *1* by a spark

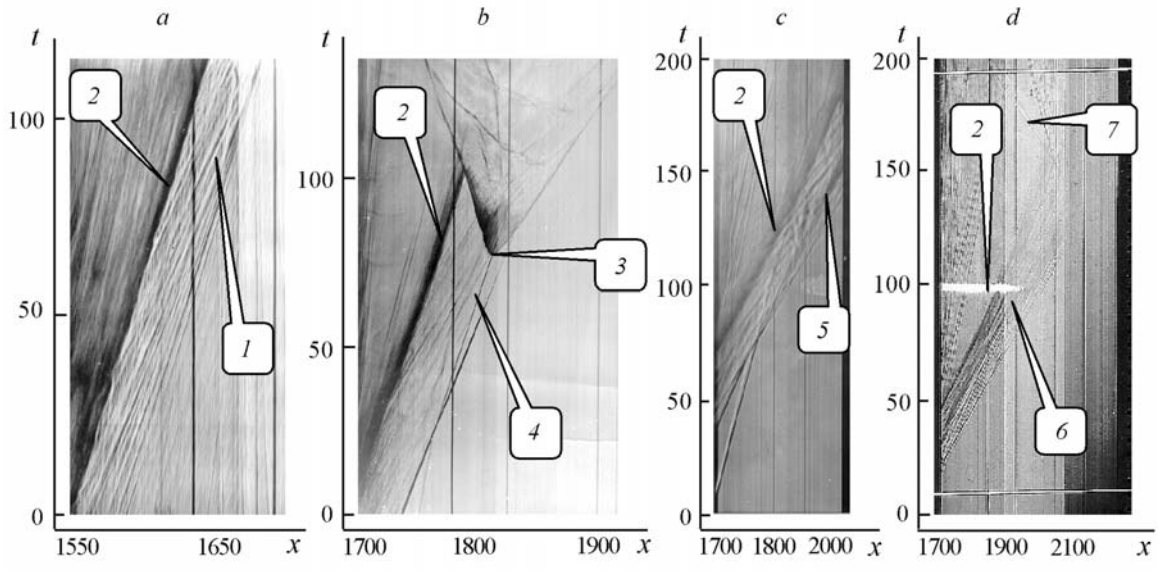

Fig. 2. Schlieren pictures illustrating the variety of DDT scenarios: a) compression waves ahead of an accelerating turbulent flame; b) the onset of detonation ahead of turbulent flame on a contact discontinuity; c) autoignition in a hot spot ahead of the flame, giving birth to a new flame zone; d) autoignition in a number of hot spots ahead of the flame. *t*, μs; *x*, mm.

plug *5*. The gas flow induced by the flame expansion was highly turbulized due to the geometry of the vessel: a toroidal vortex appeared in cavity *2,* causing a rapid expansion of the flame area on entering the second cavity. The increase in pressure in both cavities kept the valve *6* closed. Expansion of the reaction products into the narrow tube *7* produced an additional piston effect, thus increasing the flame acceleration and promoting the DDT.

The schlieren pictures illustrating the variety of scenarios of the transition process in tubes with cavities have been published before [19, 28]. Figure 2a–d illustrates the types of flow structure at different distances from the initiating section in tubes filled with methylenecyclopropane–air stoichiometric mixtures. The flame is propagating from left to right, time increasing from bottom to top. Thus, the schlieren pictures give the *x*–*t* diagrams of the process. The *x*-axis gives the actual coordinate along the axis of the tube (valve *6* was assigned to be the zero point). The *t*-axis provides only the time scale but not the actual point (the zero point is adjusted to the beginning of the registration).

Figure 2a shows the flow structure before the onset of detonation. The presence of turbulizing cavities contributes to flow irregularity ahead of the flame, which could promote the onset of detonation. The piston effect of the expanding reaction products formed on burning out the mixture in the cavities brings about the formation of several primary shock waves propagating in front of the turbulent flame. Other shock waves were formed by coalescing compression waves due to acceleration of the turbulent flame. The flame velocity is 950 m/s. The later shock waves overtake the primary ones until a strong shock wave supported by the flame-induced compression waves is formed ahead of the flame (Fig. 2b–d).

The detonation wave occurs after ignition in local exothermic centers ("hot spots") ahead of the flame. The transition scenario illustrated in Fig. 2b is characterized by the hot spot formation in the high enthalpy zone on the contact surface resulting from the interaction of two primary shock waves. Figure 2c illustrates the transition scenario characterized by the formation of a secondary combustion zone between the flame and the leading shock due to autoignition in a local exothermic center. The combustion zone expands in all directions, and the onset of detonation takes place 180 μs later. Figure 2d illustrates the transition scenario under which ignition takes place subsequently in a number of hot spots ahead of the flame. Those ignitions do not lead directly to the formation of detonation waves. Flames propagating in all directions from the ignition centers expand in both directions, leading to the formation of volume combustion and further compression of the mixture behind the leading shock. The detonation wave arises in one of the subsequent exothermic centers more closely to the leading shock beyond the limits of the photographic zone. The retonation wave moving backward at a speed of 1350 m/s in the upper part of Fig. 2d testifies to that. Analysis of the

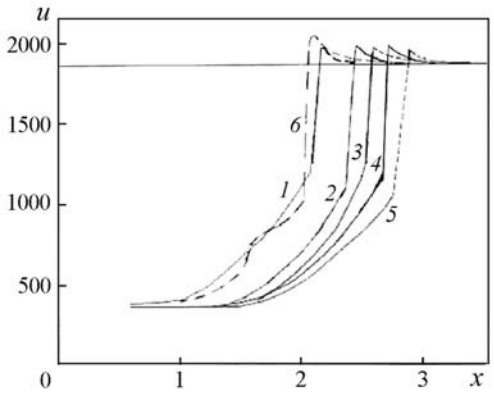

Fig. 3. Velocity of the leading disturbance variation versus length for gasoline at different values of T_0 and L_b/L_c: 1) gasoline A-76, T_0 = 350 K, L_b/L_c = 1; 2) A-76, 290 K, 0.5; 3) A-76, 290 K, 1; 4) A-76, 290 K, 0.3; 5) A-92, 290 K, 1. Dashed curve 6 corresponds to results of numerical simulations for the model hydrocarbon kinetics at C_{fuel} = 0.014, T_0 = 353 K, L_b/L_c = 1. u, m/s; x, cm.

experiments shows that detonation onset takes place in one of the exothermic centers ("hot spots") originating stochastically in the compressed gas between the leading shock and the flame zone. Depending on the hot-spot local structure, combustion could give birth to either detonation or deflagration waves propagating from the hot spot.

Experimental investigations of the device (Fig. 1) working in a pulse detonating mode were performed using internal combustion engine gasoline as a fuel and atmospheric air as an oxidant. Two types of fuel were used, characterized by different octane numbers: A-76 and A-92. For the air–gasoline gaseous mixture, introducing cavities in the ignition section allowed us to shorten the distance between the ignition point and the onset of the detonation wave (the predetonation length) down to 1.5–2.0 m in tubes 22 mm in diameter. For the same mixtures, the onset of detonation did not take place in a tube 4 m long without cavities in the ignition section. Introducing one cavity brought about the onset of detonation (predetonation length below 2.0 m), but the irregularity of the DDT process did not allow the device to work in a pulse detonating mode. With two cavities a stable cyclic mode of operation was attained with a frequency of 5–7 Hz.

The diameters of the two chambers were 100 mm each, while the length of the chambers L_c could be varied. The length of the bridge connecting the two chambers was L_b = 50 mm, and its diameter was 22 mm.

Figure 3 shows the velocity of the leading disturbance variation versus tube length in the DDT process in a long tube incorporating two cavities in the ignition section. Increasing the octane number of gasoline from 76 to 92 brought about a 15–20% increase in the predetonation length. As is seen, the dependence of detonation run-up distance on chamber length is not monotonic: the minimal distance for the present configuration occurred for the case $L_b/L_c = 0.5$.

For low temperatures, the DDT process was more stable for enriched mixtures (ϕ = 1.1), while for T > 320 K the DDT in lean mixtures (ϕ = 0.9) was also very stable.

Physical and Mathematical Models. At present, there exist three basic approaches to DDT modeling and simulation. First, its direct numerical simulation based on Navier–Stokes equations for chemically reacting mixtures, which manifests an instability considered to simulate flow turbulence (see the review paper of Oran and Gamezo, 2007 and sources referred to in [55]). The difficulty of such modeling, especially in 3-D, brought researchers to the necessity of limiting their chemistry simulation to one single-stage reaction. It was still impossible to simulate directly DDT caused by flame-induced turbulence, which limited researchers to simulating the third (intermediate) regime of detonation initiation: activating DDT by a secondary shock wave colliding flame zone [55]. Moreover, such models could not take into account subgrid turbulence, which often brings about simulation results that are in conflict with experiment. As mentioned in [55], problems of hot-spot formation and DDT sensitivity to the main gas characteristics, initial temperature, pressure, and geometry of the channel were still unresolved and could be a separate research project.

Another approach uses simplified quasi-one-dimensional models [72] and semi-empirical models. A typical example of the latter is the supposition on the proportionality of the turbulent-flame area and velocity to the distance

from the ignition location [73]. With theoretical allowance for the present statement, infinite velocity growth is cut on reaching the Chapman–Jouguet value, which permits evaluating predetonation length. The empirical model [73] is unable to match experiments in detail, as it predicts continuous acceleration, while in reality there is a velocity jump in time and space present up to an overdriven mode, and then successive slowing-down to the Chapman–Jouguet regime. Nevertheless, even simplified models supported by the proper choice of empirical parameters could be used for engineering applications.

There also exists a third approach, which unifies direct numerical simulations with the use of integral turbulence models of *k-epsilon* or *k-omega* type [28, 39, 56–58]. The advantages of such an approach lie in the possibility of using a more detailed kinetic mechanism due to the decrease in the spatial-grid resolution, which is permitted by the use of additional transport equations describing the birth, transport and decay of turbulent energy, including the subgrid level. This approach makes it possible to perform direct simulation of DDT beginning from mild ignition, through further flame acceleration due to induced turbulence and leading shock acceleration, and up to detonation onset in a hot spot. Thus will concentrate our attention on the last approach.

Numerical investigations of DDT processes were performed using a system of equations for the gaseous phase obtained by Favre averaging of the system of equations for multicomponent multiphase media. The modified *k-epsilon* model was used. To model temperature fluctuations, a third equation was added to the *k-epsilon* model to determine the mean-squared deviate of temperature [39]. The production and kinetic terms were modeled using the Gaussian quadrature technique [52]. The governing equations for the averaged values of parameters appear as follows:

$$\partial_t \rho + \nabla\cdot(\rho\mathbf{u}) = 0\,, \tag{1}$$

$$\partial_t (\rho Y_k) + \nabla\cdot(\rho\mathbf{u}Y_k) = -\nabla\cdot\mathbf{I}_k + \dot{\omega}_k\,, \tag{2}$$

$$\partial_t (\rho\mathbf{u}) + \nabla\cdot(\rho\mathbf{u}\otimes\mathbf{u}) = \rho\mathbf{g} - \nabla p + \nabla\cdot\tau\,, \tag{3}$$

$$\partial_t (\rho E) + \nabla\cdot(\rho\mathbf{u}E) = \rho\mathbf{u}\cdot\mathbf{g} - \nabla\cdot p\mathbf{u} - \nabla\cdot\mathbf{I}_q + \nabla\cdot(\tau\cdot\mathbf{u})\,. \tag{4}$$

Equations (1)–(4) include mass balance in the gas phase, mass balance of the kth component, momentum balance, and energy balance, respectively. We have the following relationships between the terms in Eqs. (1)–(2): $\sum_k Y_k = 1$, $\sum_k \mathbf{I}_k = 0$, $\sum_k \dot{\omega}_k = 0$. The state equations for the gaseous mixture are the following: $p = R_g\rho T\sum_k Y_k/W_k$, $E = \sum_k Y_k(c_{vk}T + \ + h_{0k}) + \frac{\mathbf{u}^2}{2} + k$. The turbulent heat flux $\mathbf{I}_q$ in Eq. (4) is the sum of two terms: $\mathbf{I}_q = \mathbf{J}_q + \sum_k (c_{pk}T + h_{0k})\mathbf{I}_k$, where $\mathbf{J}_q$ could be interpreted as the turbulent conductive heat flux. The eddy kinematic viscosity ν^t is expressed according to the *k-epsilon* model as $C_\mu(k^2/\varepsilon)$. The turbulent fluxes were modeled in the following way:

$$\tau = (\mu + \rho\nu^t)\,(\nabla\mathbf{u} + \nabla\mathbf{u}^T - (2/3)\,(\nabla\cdot\mathbf{u})\,U) - (2/3)\,\rho kU\,, \tag{5}$$

$$\mathbf{I}_k = -\rho\left(D + (\nu^t/\sigma_d)\right)\nabla\cdot Y_k\,,\quad \mathbf{J}_q = -\left(\lambda + \sum_k c_{pk}Y_k\rho\,(\nu^t/\sigma_t)\right)\nabla\cdot T\,. \tag{6}$$

The kth-component mass origination rate $\dot{\omega}_k$ was calculated as the sum of mass production rates ω_{kj} in each nth chemical reaction taking place in a gaseous phase. The term responsible for chemical transformations $\dot{\omega}_k$ is very sensitive to temperature variations, as it is usually an Arrhenius-law-type function for the reaction rates. Let us regard

the temperature as a stochastic function T with mean $\overline{T}$ and mean-squared deviate $\theta = \overline{T'T'}$. Then the mean value of a function having T as an independent variable could be determined as follows:

$$\overline{f(T)} = \int f\left(\overline{T} + \zeta\sqrt{\theta}\right) P_{\mathrm{d}}(\zeta)\, d\zeta ,$$

where ζ is a random value with zero expectation and unit deviate; its probability density function is $P_{\mathrm{d}}(\zeta)$. To estimate the integral, the Gaussian quadrature technique [52] is applied, using the minimal number of terms (namely, three) and assuming $P_{\mathrm{d}}(\zeta)$ to be even [39]. In this case, the formula for $f(T)$ averaging is

$$\overline{f(T)} = \frac{1}{2\chi^2} f\left(\overline{T} - \chi\sqrt{\theta}\right) + \left(1 - \frac{1}{\chi^2}\right) f(\overline{T}) + \frac{1}{2\chi^2} f\left(\overline{T} + \chi\sqrt{\theta}\right) .$$

The value of χ is of the order of 1; it depends on the particular type of probability distribution function. In the case of a normal (Gaussian) deviate, it is equal to $\sqrt{3}$ (Gauss–Hermite case) [39, 52]. Therefore, the formula above could be transformed as follows:

$$\overline{f(T)} = \frac{1}{6} f\left(\overline{T} - \sqrt{3\theta}\right) + \frac{2}{3} f(\overline{T}) + \frac{1}{6} f\left(\overline{T} + \sqrt{3\theta}\right) .$$

Assume that the probability density function of Gaussian type is a first-order approximation. Approximations of higher orders should incorporate assumptions on the deviation of the function from Gaussian form. In our case, the function $f(T)$ is the Arrhenius temperature dependence; the whole average for $\dot{\omega}_k$ is constructed using combinations of these dependences. Averaged magnitudes for mass fractions and density were used in the Arrhenius law for $\dot{\omega}_k$, as the dependence of these functions is not as strong as the dependence of temperature.

The model was then closed by the equations for k, θ, and ε:

$$\partial_t(\rho k) + \nabla\cdot(\rho\mathbf{u}k) = \nabla\cdot\left((\mu + \rho(\nu^t/\sigma_k))\nabla k\right) + \tau^t : \nabla\mathbf{u} - \rho\varepsilon , \tag{7}$$

$$\partial_t(\rho\varepsilon) + \nabla\cdot(\rho\mathbf{u}\varepsilon) = \nabla\cdot\left((\mu + \rho(\nu^t/\sigma_\varepsilon))\nabla\varepsilon\right) + (\varepsilon/k)\left(C_{1\varepsilon}\tau^t : \nabla\mathbf{u} - C_{2\varepsilon}\rho\varepsilon\right) , \tag{8}$$

$$\partial_t(\rho c_p\theta) + \nabla\cdot(\rho\mathbf{u}\tilde{c}_p\theta) = \nabla\cdot\left(\left(\lambda + \sum_k c_{pk}Y_k\rho\left(\nu^t/\sigma_k\right)\right)\nabla\theta\right) + P_\theta + W_\theta - D_\theta , \tag{9}$$

where the production terms P_θ and W_θ and the dissipation term D_θ were determined by the following formulas:

$$P_\theta = 2\rho\sum_k c_{pk}Y_k\left(\nu^t/\sigma_k\right)(\nabla T)^2 , \quad W_\theta = -\sum_k \overline{\omega_k' T'}\, h_{0k} , \quad D_\theta = C_{\mathrm{g}}\rho\sum_k c_{pk}Y_k\frac{\varepsilon}{k}\frac{\theta}{\theta_{\mathrm{m}} - \theta} , \quad c_p = \sum_k c_{pk}Y_k . \tag{10}$$

In deriving the production W_θ due to chemical reactions, the Arrhenius law for chemical transformations was assumed. To calculate the averaged term $\dot{\omega}_k$, the Gaussian quadrature technique was applied [39, 52]:

$$\overline{T'A(T)} = \theta\frac{A(\overline{T} + \sqrt{3\theta}) - A(\overline{T} - \sqrt{3\theta})}{2\sqrt{3\theta}} . \tag{11}$$

The dissipation function D_θ was chosen in the form of (10) to satisfy the rule that the squared temperature deviate cannot exceed its maximal possible value θ_{m}, because the value of $T = \overline{T} + T'$ cannot be negative. However, production terms do not grant the presence of such a boundary. To guarantee it, we incorporate the multiplier $1/(\theta_{\mathrm{m}} - \theta)$ into the dissipation term (the other multipliers are standard, see [41]). In order to estimate the value of θ_{m}, we should take into account that the probability for the deviate value to be twice the mean deviate value is less than 1% for the normal

distribution [53]. Also, we should take into account that the mean temperature deviate in experiments published by Philip [41] did not exceed half the maximal mean temperature. With this, we estimate θ_m as follows: $\theta_m = \overline{T}^2/4$. The dissipation constant C_g in (13) can be determined based on the experiments [41]: $C_g = 2.8$.

The constants in (7)–(10) take the following standard values:

$$C_\mu = 0.09\,, \quad C_{1\varepsilon} = 1.45\,, \quad C_{2\varepsilon} = 1.92\,,$$

$$\sigma_d = 1\,, \quad \sigma_t = 0.9\,, \quad \sigma_k = 1\,, \quad \sigma_\varepsilon = 1.3\,, \quad \theta_m = \overline{T}^2/4\,, \quad C_g = 2.8\,.$$

The gaseous phase was assumed to contain the following set of species: O_2; C_nH_m; CO_2; H_2; H_2O; N_2.

We considered a model hydrocarbon fuel. The present model allowed us to vary the hydrocarbon composition and chemical potential, being a function of the composition. The chemical potential of hydrocarbon fuel h_2^0 was considered to be a problem parameter, along with its composition n and m. The potential depends not only on n and m but also on the particular hydrocarbon fractions of which the fuel consists. The following brutto reactions between the species were considered:

$$C_nH_m + \left(\frac{n}{2} + \sigma\,\frac{m}{4}\right)O_2 \to nCO + \sigma\,\frac{m}{2}\,H_2O + (1-\sigma)\,\frac{m}{2}\,H_2\,,$$

$$CO + 0.5O_2 \to CO_2\,,$$

$$CO_2 + M \to CO + 0.5O_2 + M\,,$$

$$H_2 + 0.5O_2 \to H_2O\,,$$

$$H_2O + M \to H_2 + 0.5O_2 + M\,.$$

Here, σ is the share of water in the hydrocarbon decomposition. This parameter depends on the particular content of the fuel (like the hydrocarbon chemical potential). We denote $B = 5$ — the number of reactions. The rates of species origination are assumed to yield the Arrhenius law and the law of acting masses. With multiple reactions, the origination rates are split into elementary parts:

$$\dot{\omega}_k = \sum_{j=1}^{B} \omega_{kj}\,, \tag{12}$$

where ω_{kj} is the kth species origination rate per volume due to the jth reaction. The actual formulas for determining ω_{kj} for the present reaction mechanism are described in [39].

The temperature deviation production term in Eq. (9) for multiple species and reactions has the following form:

$$W_\theta = -\,\overline{T'\sum_{j=1}^{B}\sum_{k=1}^{K} h_k^0 \dot{\omega}_{kj}}\,. \tag{13}$$

Each term ω_{kj} incorporates the Arrhenius function for the jth reaction $A_j(T)$, which is assumed to have the following form:

$$A_j(T) = \begin{cases} K_j \exp\left(-\dfrac{T_{aj}}{T}\right), & T \ge T_{mj}\,; \\ 0\,, & T < T_{mj}\,, \end{cases} \tag{14}$$

where K_j is the pre-exponential factor, T_{aj} is the activation temperature, and T_{mj} is the minimum temperature, for which the actual reaction velocity is zero. The Arrhenius function provides an ideal formula, following which one obtains final reaction rates for all temperatures above absolute zero and, consequently, comes to the conclusion that sooner or later all mixtures would come to equilibrium. However, the presence of small losses and other factors not taken into account by simplified models permit mixtures to exist in metastable states for infinitely long times. The minimal temperature introduced in our model characterizes the upper-limit temperature of a meta-stable mixture. The choice of this temperature could be dependent on the characteristic times for the problem. In order to obtain the term W_θ (13), one should find the mean values $\overline{T'A_j(T)}$ using formula (11) and then sum up those terms using formula (13). The procedure for averaging nonlinear functions was described in detail in [39].

The boundary of the computational domain contains the outer walls and the axis of symmetry. The walls for the case of cylindrical symmetry could be a combination of coaxial cylindrical surfaces and rings or plates orthogonal to the axis.

The boundary conditions for the gas phase are constructed in accordance with the following considerations: the walls of the cylindrical domain are thermally insulated and noncatalytic, the velocity of the gas is zero on the walls, and the averaged gas motion has cylindrical symmetry. This leads to von Neumann's conditions for temperature and mass fractions of species at the walls of the cylinder (their normal derivatives are equal to zero):

$$x = 0\,,\ \ x = x_i\,,\ \ r_i \le r \le R_i:\ \ u_x = u_r = 0\,,\ \ \frac{\partial T}{\partial x} = 0\,,\ \ \frac{\partial Y_k}{\partial x} = 0\,; \qquad (15)$$
$$x = X\,,$$

$$r = R_i\,,\ \ x_i \le x \le x_{i+1}\,,\ \ r = r_i\,,\ \ x_{i-1} \le x \le x_i;\ \ i = 1, ..., N-1\,,\ \ \ u_x = u_r = 0\,,\ \ \frac{\partial T}{\partial r} = 0\,,\ \ \frac{\partial Y_k}{\partial x} = 0\,; \qquad (16)$$

$$r = 0\,,\ \ 0 \le x \le X:\ \ u_r = 0\,,\ \ \frac{\partial u_x}{\partial r} = 0\,,\ \ \frac{\partial T}{\partial r} = 0\,,\ \ \frac{\partial Y_k}{\partial r} = 0\,. \qquad (17)$$

The boundary conditions for turbulent parameters k, ε, and θ are constructed according to the wall laws [28]:

$$k = 0\,,\ \ \frac{\partial \varepsilon}{\partial \mathbf{n}} = 0\,,\ \ \frac{\partial \theta}{\partial \mathbf{n}} = 0\,, \qquad (18)$$

where $\mathbf{n}$ is the normal vector to the wall. To take into account the wall damping effect, the coefficients of the original turbulence model are modified in accordance with the Lam–Bremhorst low-Reynolds models [42]:

$$C_\mu = C_\mu^0 f_\mu\,,$$
$$C_{1\varepsilon} = C_{1\varepsilon}^0 f_1\,,$$
$$C_{2\varepsilon} = C_{2\varepsilon}^0 f_2\,, \qquad (19)$$

where f_μ, f_1, and f_2 are positive functions ($0 < f_\mu \le 1, f_1 \ge 1, 0 \le f_2 \le 1$), which depend on two local Reynolds numbers

$$R_t = \frac{k^2}{\nu\varepsilon}\,,\ \ R_y = \sqrt{k}\,\frac{y}{\nu}\,, \qquad (20)$$

where y is the distance from the nearest wall. For the Lam–Bremhorst low-Reynolds k–ε model the functions are determined in the following way:

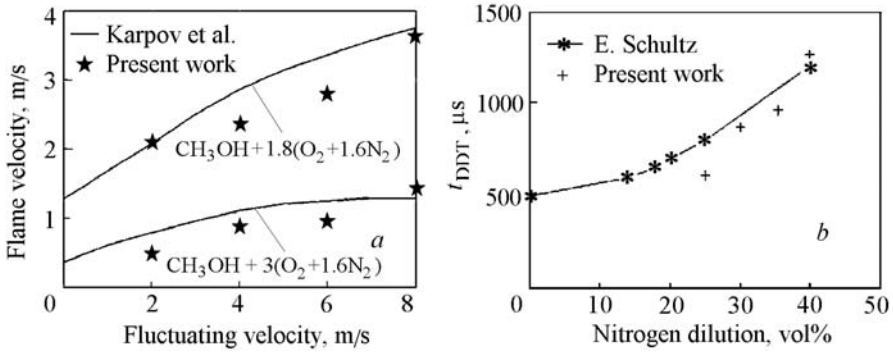

Fig. 4. Comparison of numerical results of the present paper and experimental results for flame velocity versus turbulent velocity fluctuations [a: 1) $\alpha = 1.2$, 2) $\alpha = 2$] and predetonation time in a hydrogen–oxygen mixture as a function of nitrogen dilution (b).

$$f_\mu = [1 - \exp(-0.0165R_y)]^2 \left(1 + \frac{20.5}{R_t}\right),$$

$$f_1 = 1 + \left(\frac{0.05}{f_\mu}\right)^3,$$

$$f_2 = 1 - \exp\left(-R_t^2\right).$$

Numerical Model and Validating Experiments. The system of gas-dynamics equations rewritten in vector form was split into three parts due to three different physical processes: chemistry, source terms, and generalized turbulence production terms formed the "local part" of the equations; convective terms formed the "hyperbolic part" of the equations; and diffusive, viscous, and thermo-conductive terms formed the "parabolic part" of the equations.

The local part was solved implicitly using an iterative algorithm independently for each grid node. The hyperbolic part was solved using explicit FCT techniques [43]. The parabolic part was solved implicitly using 3-diagonal matrix solvers for linear equations [44]. The techniques removed viscosity from the time-step criterion and reduced it to the Courant–Friedrichs–Lewy criterion.

To solve the system of equations, splitting by coordinates was used according to MacCormack [45].

Following the symmetry of boundary conditions, simulations were performed for a 2-D cylindrical grid. The detonation wave structure is essentially 3-D. Thus, one should not expect 2-D simulations to provide detailed matching in terms of microstructure of the detonation front. However, these simulations allow one to develop macroscopical characteristics of the phenomenon.

Verification of the numerical scheme was performed by comparing the results of test runs with the exact gas-dynamics solutions and with model experiments on turbulent-flame propagation in confined volumes.

The mathematical models for simulating turbulent-flame acceleration and onset of detonation in a chemically reacting gas were validated by comparing the results of numerical simulations for flame propagation in turbulized gaseous combustible mixtures with results of experiments [50], which provided the dependence of turbulent-flame-propagation velocity as a function of flow turbulence and mixture composition.

The initial values for turbulent kinetic energy and dissipation were introduced to simulate initial flow turbulization prior to ignition. The mean flow velocity was assumed to be zero. The two-dimensional problem of flame propagation in a tube of constant cross section filled with $CH_3OH + 1.5\alpha(O_2 + 1.6N_2)$ gaseous mixture was considered. The kinetic mechanism was based on the one suggested in [51] and incorporated 129 elementary stages. The results were compared with experimental observations summarized in [50].

Results of numerical simulations showed that the flame-propagation velocity was nearly constant and relatively small at the beginning of the process, but then it rapidly increased, presumably due to self-turbulization effects. Thus,

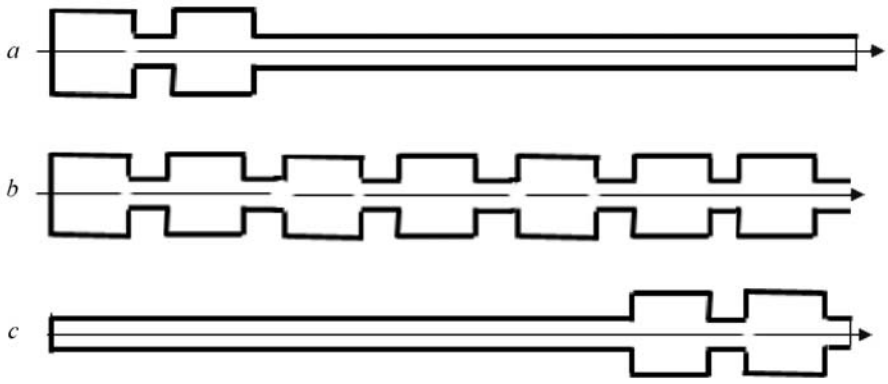

Fig. 5. Geometry of the computational domain: a) two cavities in the ignition section; b) cavities incorporated into the tube along the whole length; c) two cavities in the far-end section of the tube.

the calculated velocity just before flame acceleration could serve as reference data for comparison with experimental measurements [50].

Figure 4a illustrates the experimental dependence of turbulent-flame velocity on flow turbulence (solid curves provided in [50]) for two mixture compositions: $\alpha = 1.2$ and 2.0. Flame velocities obtained in processing the results of our numerical simulations for both mixture compositions and different levels of turbulence are shown by stars in Fig. 4a.

Figure 4b illustrates the experimental dependence of predetonation time in DDT in hydrogen–oxygen mixtures as a function of nitrogen dilution of the mixture [54]. Numerical simulations [56, 57] performed for validating purposes used the kinetic mechanism suggested in [74]. The predetonation times obtained in our numerical simulations for four different values of nitrogen content are shown by dots. Comparison of the results illustrates good agreement between theoretical calculations and experimental data.

For further numerical simulations, a simpler kinetic model, described in the present paper and simulating a model hydrocarbon fuel, was used. Numerical modeling was performed with an initial low level of turbulence. That allowed shortening the calculation time without any harm to precision. Numerical simulations described above showed that after mixture ignition the system quickly "forgot" about the initial level of turbulence due to flow-induced turbulence in a complex confined geometry.

Figure 3 contains a dashed curve illustrating numerical results obtained for the velocity of the leading disturbance for DDT at the elevated temperature T_0 = 353 K. The location of the leading disturbance in numerical simulations was tracked as the location of the first maximal absolute value of the negative pressure gradient:

$$x = \sup\left\{x : \min\frac{\partial p}{\partial x}\right\}.$$

Comparison of results with experimental data provides satisfactory agreement.

Numerical Investigations. In numerical simulations, the test vessel contained a detonation tube with a number of cavities of wider cross section incorporated in different places of the tube filled with a combustible gaseous mixture at ambient pressure (Fig. 5). Ignition of the mixture was performed by a concentrated energy release in the center of the first cavity or in the tube itself on the left-hand side near the closed end. The number of cavities was varied from one to twenty. The location of the cavities was also a question under investigation. Simulations were performed for the following cases:

1) the initial section had two incorporated turbulizing cavities of a wider cross section;
2) the far-end section had two similar incorporated turbulizing cavities of a wider cross section;
3) turbulizing cavities were located along the whole tube.

The ratio of tube/cavity cross-section areas was also a parameter under investigation. The values of the main problem parameters adopted for numerical experiments are given in Table 1 in SI units.

Additional validation of the code was performed by calculating the parameters for the self-sustained Chapman–Jouguet detonation in the model gaseous mixture under consideration. The results shown in Table 2 provide theo-

TABLE 1. Values of the Main Parameters in SI Units

Parameter	Value
Tube section dimension along X	2.150
Initial pressure	$1.013 \cdot 10^5$
Initial temperature	$3 \cdot 10^2$
Initial temperature deviate	1
Initial turbulent energy	0.1
Initial characteristic length of turbulence	0.0050
Initial volumetric share of O_2	0.2200
Init. vol. share of CNHM	0.0150
Init. vol. share of H_2	0
Init. vol. share of H_2O	0
Init. vol. share of CO_2	0
Init. vol. share of CO	0
Init. vol. share of N_2	0.7800
Chemical potential of O_2	0
Chem. potent. of CNHM	$-1.34 \cdot 10^5$
Chem. potent. of H_2	0
Chem. potent. of H_2O	$-2.395 \cdot 10^5$
Chem. potent. of CO_2	$-3.92 \cdot 10^5$
Chem. potent. of CO	$-1.105 \cdot 10^5$
Chem. potent. of N_2	0
Carbon in CNHM	10
Hydrogen in CNHM	22
Water share in CNHM decomposition	0.2
Pre-exponential factor: methane decomposition	10^9
Activation temperature: CNHM + $O_2 \rightarrow$ CO+H_2	$2.527 \cdot 10^4$
Minimal temperature: CNHM + $O_2 \rightarrow$ CO+H_2	$5 \cdot 10^2$
Pre-exponential factor: hydrogen burning	$7 \cdot 10^7$
Activation temperature: $H_2 + O_2 \rightarrow H_2O$	$1.0614 \cdot 10^4$
Minimal temperature: $H_2 + O_2 \rightarrow H_2O$	$6 \cdot 10^2$
Pre-exponential factor: water pyrolise	$8.7 \cdot 10^7$
Activation temperature: $H_2O \rightarrow H_2 + O_2$	$3.5 \cdot 10^4$
Minimal temperature: $H_2O \rightarrow H_2 + O_2$	10^3
Pre-exponential factor: carbon mono-oxide burning	$5.89 \cdot 10^6$
Activation temperature: $CO + O_2 \rightarrow CO_2$	$1.0614 \cdot 10^4$
Minimal temperature: $CO + O_2 \rightarrow CO_2$	$6 \cdot 10^2$
Pre-exponential factor: carbon dioxide pyrolisis	$2.75 \cdot 10^7$
Activation temperature: $CO_2 \rightarrow CO + O_2$	$2.0418 \cdot 10^4$
Minimal temperature: $CO_2 \rightarrow CO + O_2$	10^3
Total ignition energy	2
Ignition time	10^{-4}
Ignition X position	$5 \cdot 10^{-2}$
Ignition ball radius	10^{-2}

retical data for detonation velocity as a function of fuel concentration. Velocities obtained as results of numerical simulations of unsteady-state problems using the developed code are provided along with their fluctuations.

Analyzing the results obtained for the detonation velocity, one can note that the maximal velocity is attained for a fuel concentration higher than the stoichiometric one for the model hydrocarbon fuel considered. The cell size for this model fuel at a pressure of 1 bar and $\dot{O}_0$ = 300 Ê was 4–8 mm for $C_{\text{fuel}} = 0.015$ and 8–12 mm for $C_{\text{fuel}} = 0.012$.

The grid resolution was sufficient for the detonation velocity to be insensitive to further grid refinement (1 mm grid size). The Chapman–Jouguet detonation structure obtained numerically was in good coincidence with the

TABLE 2. Theoretical and Numerically Obtained Data for Detonation Velocity

Fuel concentration	Detonation velocity, m/s	
	Obtained from numerical simulations	Theoretical
0.009		1694.2 (lean mixture)
0.010		1744.0
0.011	1735–1790	1788.6
0.012	1840–1865	1829.1
0.013		1866.1 (below stoichiometry)
0.014	1880–1920	1900.1 (above stoichiometry)
0.015	1930–1960	1931.5
0.016		1960.5
0.017		1987.0
0.018		2010.9
0.019		2031.4
0.020		2046.6
0.021		2052.7 (detonation velocity maximum)
0.022		2047.2
0.023		2033.1 (rich mixture)

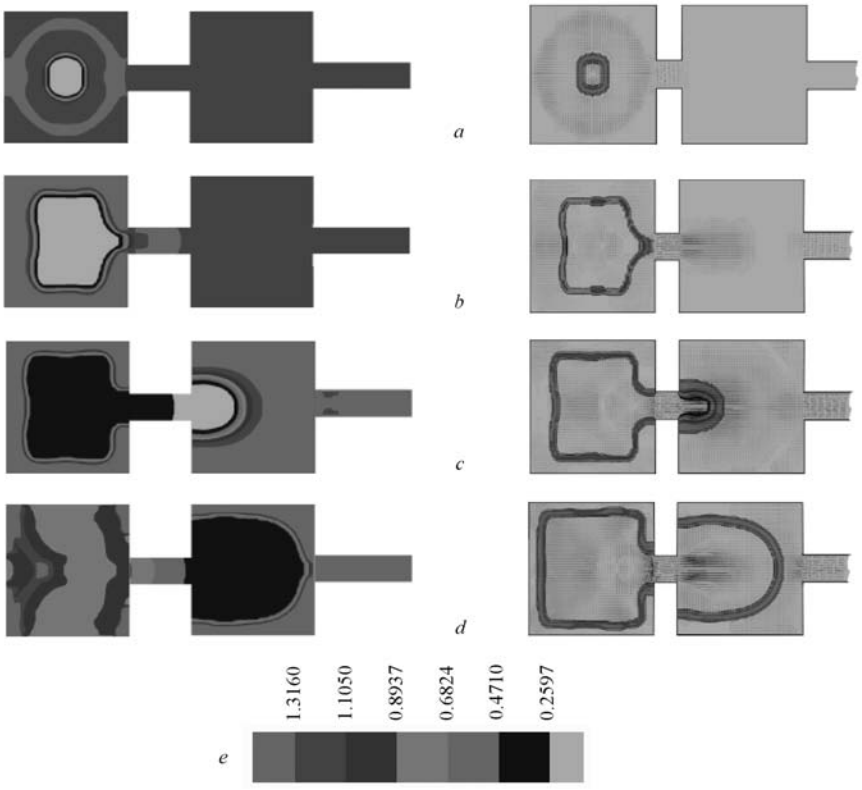

Fig. 6. Gas density (left) and reaction intensity (right) fields for successive times after ignition: a) 0.3; b) 2.7; c) 3.5; d) 4.1 ms; e) mapping colors for density (kg/m^3).

theoretical one; no signs of undercompressed weak detonation were noted, which testifies to the absence of ignition driven by numerical errors [27, 28].

The numerical simulations described below were carried out using a 2-GHz PC. The simulation time for the device incorporating 10 cavities was about 6 hours, that incorporating 20 cavities — 60 hours.

The Role of Cavities in the Ignition Section. We investigate the influence of turbulizing cavities incorporated into the ignition section of a test vessel containing a detonation tube with two cavities of wider cross section

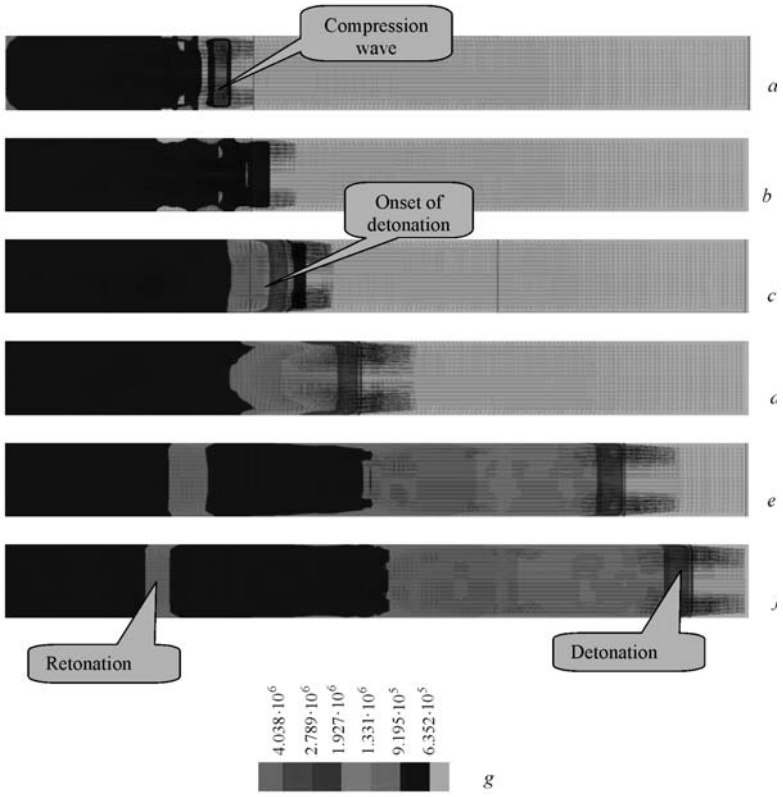

Fig. 7. Pressure evolution in the detonation tube in the transition zone for successive times: a) 4.593; b) 4.611; c) 4.628; d) 4.643; e) 4.696; f) 4.709 ms; g) mapping colors for pressure (Pa).

filled with a combustible gaseous mixture at ambient pressure. Ignition of the mixture is performed by a concentrated energy release in the center of the first cavity. The tube is 20 mm in diameter with two cavities 100 mm in diameter and 100 mm long incorporated in the ignition section. The bridge between the two cavities is 20 mm in diameter and 50 mm long. The results were obtained for the fuel molar concentration $C_{\text{fuel}} = 0.015$ (the stoichiometric concentration is $C_{\text{fuel}} = 0.014$).

The results (Figs. 6 and 7) show that on mixture ignition in the first cavity the process of flame propagation is rather slow and is determined mostly by initial turbulization of the mixture. The flame that is initially spherical changes its form to cylindrical on approaching the walls of the cavity. The flame accelerates and penetrates the bridge between the two cavities due to the gas flow caused by the expansion of reaction products. Line segments marking gas velocity show that a high-velocity jet penetrates the second cavity prior to the flame front, which brings about a very fast flame propagation both due to additional flow turbulization and the piston effect of the expanding reaction products supported by the continuing combustion in the first cavity.

Fast combustion in the second cavity brings about a sharp pressure increase that pushes the flame further into the tube (Fig. 7). A shock wave is formed in the tube ahead of the flame zone. Pressure waves generated by continuing combustion in the cavities overtake the flame and the leading shock wave. That causes nonuniformity in the combustion zone and the formation of transverse waves. At some place the detonation arises from a hot spot within the combustion zone. For the present scenario of the process, the onset of detonation takes place at a distance of about 1 m from the ignition section. Before the onset of detonation, hot spots appearing in the combustion zone bring about the formation of compression waves irradiated from the reaction zone in all directions. Those waves support the leading shock and propagate backwards as well until the onset of detonation waves in one of the successive hot spots gives birth about the strong detonation and retonation waves.

Pressure profiles along the tube axis for successive times are illustrated in Fig. 8. Vertical lines mark the location of cavities in the ignition section. It is seen from the figures that after the onset of detonation takes place in

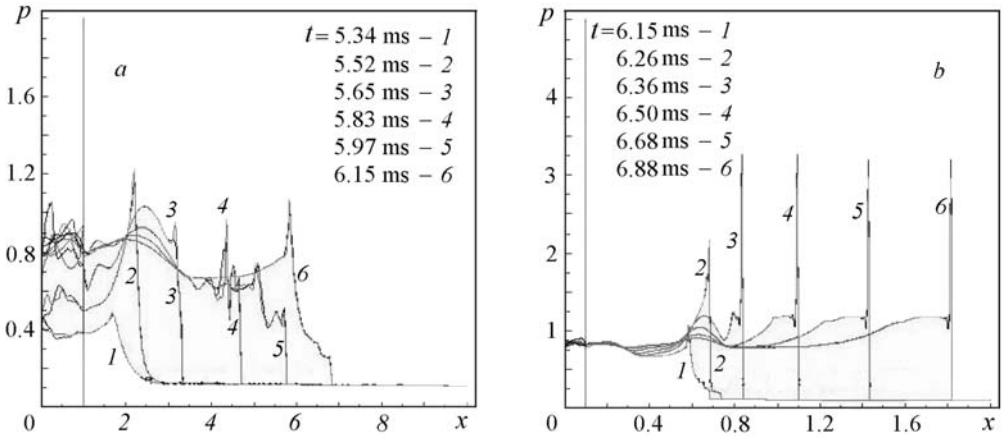

Fig. 8. Pressure profiles along the axis for successive times in a device incorporating one cavity in the ignition section at a fuel molar concentration of 0.012. p, MPa; x, m.

one of the exothermic centers, the detonation wave overtakes the leading shock. Their interaction gives birth to an overdriven detonation, which propagates forward and gradually slows down to a Chapman–Jouguet regime, and to a rarefaction wave propagating backward but being blown off by the gas flow. Thus, the pressure profile behind the detonation in DDT is the result of interaction of two rarefaction waves moving in opposite directions, which introduces some peculiarities as compared with the classical Taylor profile.

Computational experiments allowed one to explain the multiplicity of scenarios for the DDT process in gases as well as the experimentally observed phenomenon of detonation onset on the contact discontinuities in the flow ahead of the accelerating turbulent flame [27, 28]. Actually, it was observed that flame acceleration could give birth to several shock waves ahead of the flame zone, overtaking each other. In particular, upon interaction of two shock waves ahead of the flame, one leading shock is formed and also a contact discontinuity existing between the leading shock and flame zone and giving birth to a hot spot.

The onset of detonation on the contact surface being one of the most probable scenarios has the following explanation. In the case where weak shock waves precede the deflagration wave, their interaction gives birth to an advancing leading shock, rarefaction wave moving backward towards the flame front and the contact discontinuity that exists between the leading shock and the flame zone. The zone between the leading shock and the contact surface has a higher temperature. Thus, the induction period in this zone is less than that between the flame front and the contact surface. The first thermal explosion takes place in the layer of gas that has been exposed to the higher temperature for the longest time, i.e., in the gas layer on the contact surface. Depending on the flow history and induction delay gradients in the vicinity of the contact surface, this explosion can bring about either deflagration or detonation waves propagating from the exothermic center. Following the gradient mechanism, detonation waves propagating in opposite directions could be formed in this zone. The intensity of the retonation (reverse detonation) wave decreases on entering the reaction products. The detonation wave overtaking the leading shock forms an overdriven detonation in the uncompressed mixture that gradually slows down to the Chapman–Jouguet speed.

Normal deflagration waves caused by one or several successive autoignitions (thermal explosions) on contact discontinuities in the precompressed gas, which propagate in both directions from the place of origin, cause further compression and heating of the gas, thus decreasing the induction period and leading to formation of a detonation wave. Thus, the multiplicity of "hot spots" present in the flow ahead of the accelerating flame can bring about a multiplicity of scenarios of the deflagration-to-detonation transition.

Decreasing the number of cavities incorporated into the ignition section to one cavity and then to zero cavities brings about an increase in the predetonation length. In the absence of turbulizing cavities of wider cross section in the ignition zone, DDT could also take place, but it is very unstable: a small variation of parameters could strongly influence the DDT scenario. The onset of detonation in different experiments has a sporadic character.

Figure 9 illustrates flame trajectories and pressure evolution for the DDT in a tube without cavities, and with one and two cavities incorporated into the ignition section for the fuel concentration C_{fuel} = 0.012. Comparison of the

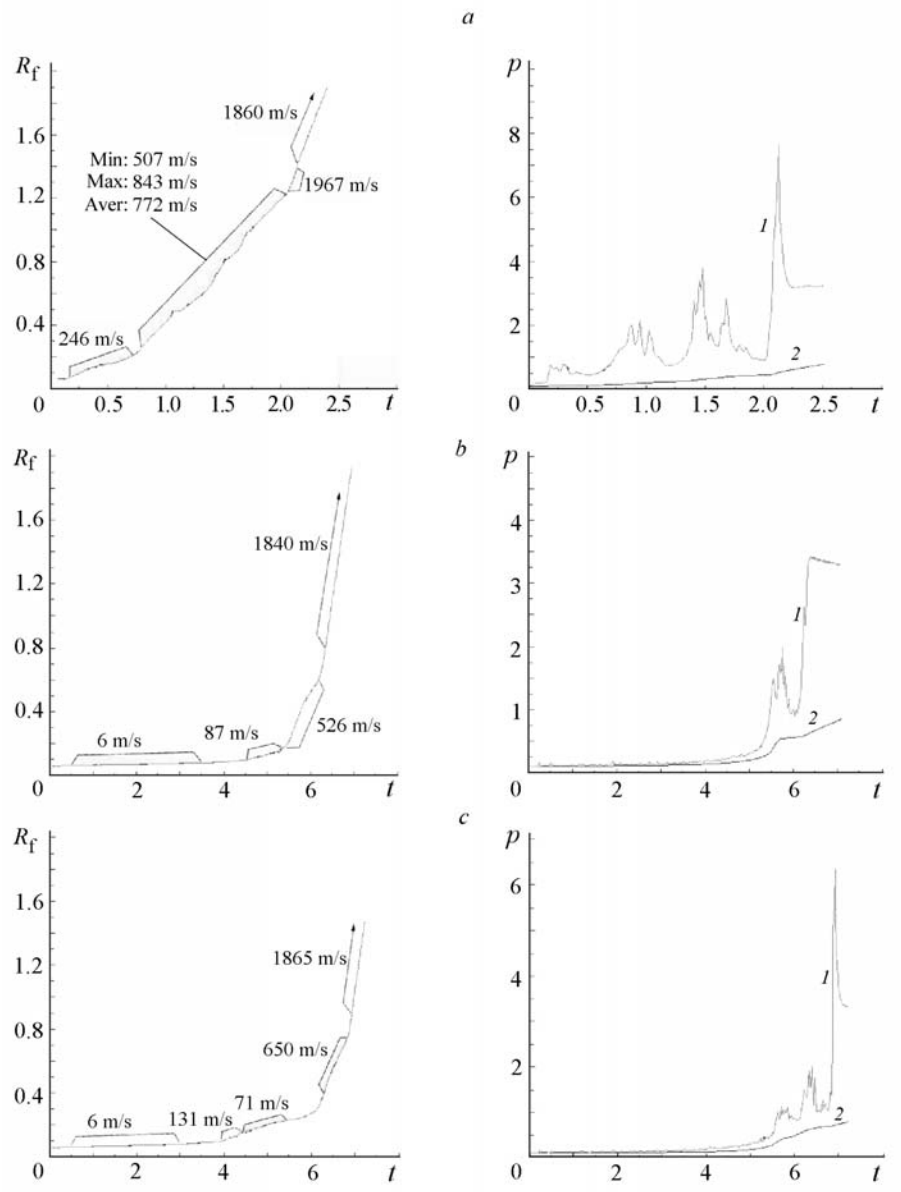

Fig. 9. Reaction-front trajectories (left) and pressure evolution (right) for DDT in a gaseous mixture in tubes at a fuel concentration of 0.012: without turbulizing cavities (a); with one (b) and two (c) turbulizing cavities incorporated into the ignition section; 1 and 2) maximal and average pressure in the device, respectively. R_f, m; p, MPa; t, ms.

velocities and trajectories shows that incorporating cavities in the ignition section promotes the DDT. Incorporating turbulizing cavities brings about a slower flame propagation in the very beginning of the process due to an increase in volume but then leads to a stable detonation initiation and its coming to a self-sustained regime, while in the absence of turbulizing cavities flame propagation is much faster and irregular in the very beginning of the process. This is due to the fact that a similar initiation energy is being redistributed within a smaller volume, thus providing an initiating piston effect, which is not strong enough to cause the onset of detonation but is sufficient to initiate an irregular galloping combustion mode. The onset of detonation takes place at a distance of 1.2 m from the beginning of the tube, which is higher than for the case of one or two cavities incorporated into the ignition section. However, shortening the run-up distance could also bring about an increase in the time for DDT and could be important in limiting the maximum PDE operating frequency.

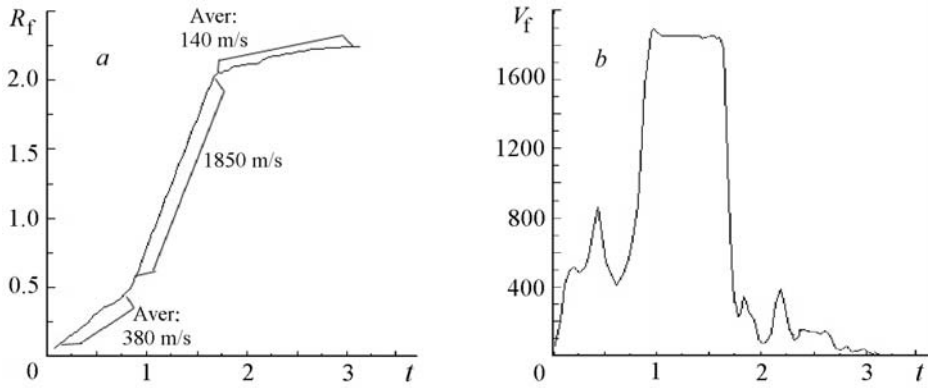

Fig. 10. Reaction-front trajectory (a) and velocity (b) in a tube incorporating two turbulizing cavities of wider cross section at the end for a fuel volumetric concentration of 0.012. R_f, m; V_f, m/s; t, ms.

Using cavities in the ignition made the transition more reproducible, which is important for PDE applications. The onset of detonation in a tube without cavities is an irreproducible stochastic process, and each pulsation of velocity depending on some additional disturbance could result in the onset of detonation. Thus, the predetonation length for such an irreproducible transition process, as we saw in a tube without cavities in the ignition section, could be less or much larger than the one obtained in the numerical experiment considered.

The Influence of Wide Cavities at the End of the Tube. To provide comparative data here we investigated the role of two cavities of wider cross section incorporated in the far end of the tube (Fig. 5c). The tube was identical to that used in numerical experiments described in the previous section, but ignition was performed at the opposite side (symmetrical with respect to 180^o rotation). To ensure detonation formation the ignition energy was 2.5 times higher than that in the above experiments. The ignition source was located at the tube axis.

Numerical results showed that after ignition in a narrow tube, acceleration of the flame zone accompanied by a number of oscillations brought about the formation of a detonation wave propagating with mean velocity 1850 m/s. On entering the first cavity, decoupling of the shock wave and reaction-zone took place and the mean velocity of reaction-zone propagation decreased to 200 m/s; then, in a narrow bridge, the flame accelerated up to 400 m/s and slowed down in the second cavity to 100 m/s. The average velocity in the cavities was 140 m/s. Decoupling of the shock wave and reaction zone took place due to the fact that the geometrical factor, which is the ratio of the critical detonation exit diameter to the original tube diameter [29], was more than unity.

Figure 10 illustrates the reaction-front velocity variation versus time for the detonation onset and degeneration in a tube with two cavities at the end. The fuel concentration in the mixture was 0.012, which corresponds to results of numerical experiments illustrated in Figs. 8 and 9.

The results show that a normal detonation wave propagating close to the Chapman–Jouguet velocity on entering a set of cavities of wider cross section degenerated to a galloping combustion mode (Fig. 10), which was characterized by a low subsonic velocity of reaction-front propagation in the axial direction.

The Influence of Fuel Concentration. Figure 11a–c shows the flame-front velocity variation in the tube for different values of fuel concentration but for one and the same tube geometry. It is seen that the flame accelerates on entering the second cavity, then it slows down. A high-speed combustion wave enters the detonation tube, where the transition takes place.

Analysis of results present in Fig. 11 shows that on decreasing the fuel content of the mixtures its detonability via DDT decreases. The predetonation time increases (Fig. 11a and b), but once the onset of detonation takes place it propagates at a practically constant velocity. Velocity diagrams indicate that in both cases the onset of detonation takes place via an overdriven regime.

A decrease in fuel molar concentration below $C_{fuel} = 0.011$ brings about the formation of galloping combustion regimes. Those galloping combustion regimes are not caused by numerical instability, as one cycle of the process develops within 150–200 time steps. The hot spots occur alternatively near the lateral walls (higher pressure peaks) and in the center and bring about flame-zone accelerations. The flame velocity shown in Fig. 11c allows one to evalu-

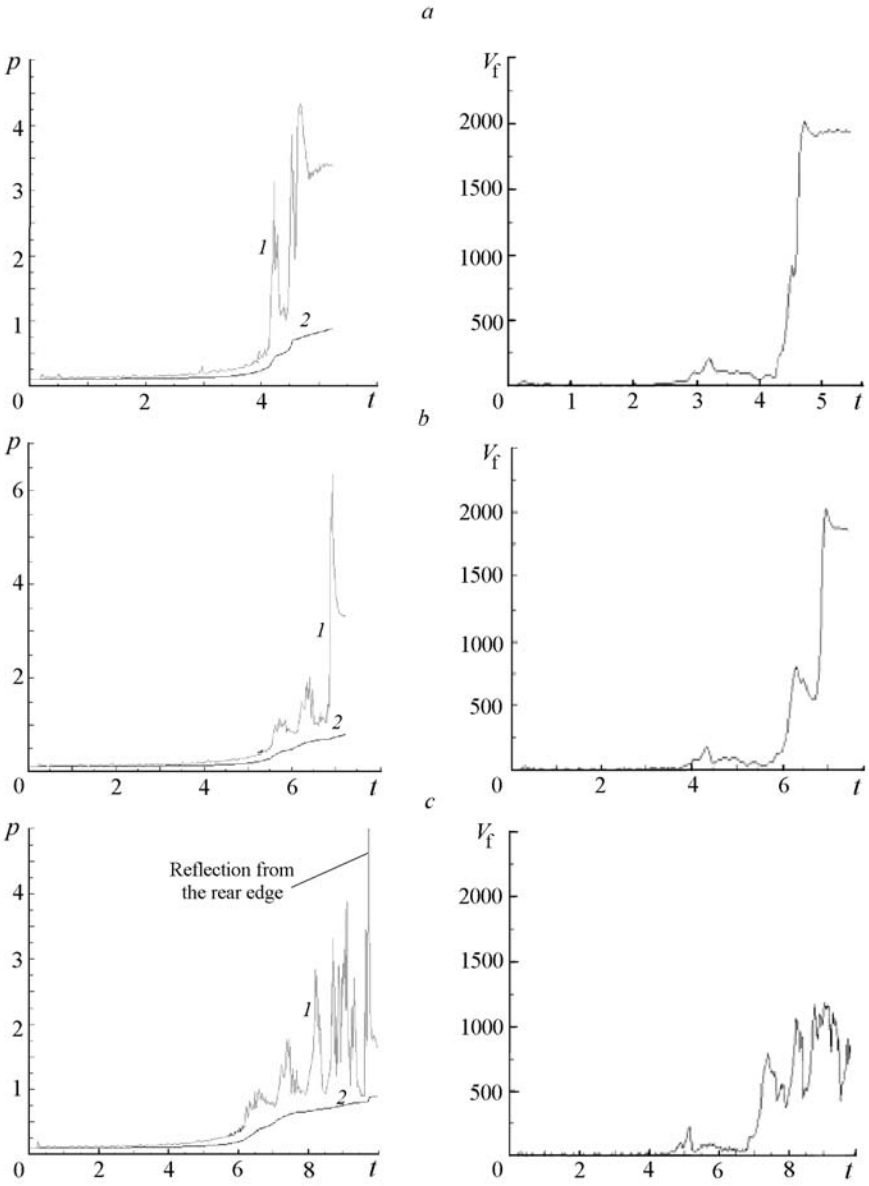

Fig. 11. Pressure and reaction-front velocity evolution in the tube incorporating two cavities in the ignition section for different fuel volume concentrations: C_{fuel} = 0.015 (a); 0.012 (b); 0.011 (c); 1 and 2) maximal and average pressure in the device, respectively. p, Mpa; V_f, m/s; t, ms.

ate oscillations. For a fuel concentration of 0.011, the galloping combustion regime propagates with velocity oscillations within the range 420–1200 m/s. The onset of detonation does not take place within the 2.25-m length of the tube. The average velocity of the galloping combustion mode here was 760 m/s.

The Influence of Wider Cavities Incorporated into the Tube along the Whole Length. The results of previous investigations showed that incorporating one or two cavities of wider cross section into the beginning of the tube, where ignition takes place, stabilizes the DDT process and shortens the predetonation length. To investigate the influence of an increase in the number of cavities on the onset of detonation, numerical experiments were undertaken for the structure (Fig. 5b) incorporating 20 similar cavities 100 mm in diameter and 100 mm long incorporated into a tube 20 mm in diameter with intervals of 50 mm. The length of the structure turned out to be 2.95 m.

The results showed that for the fuel concentration C_{fuel} = 0.012 the DDT process did not take place at all. A galloping combustion mode was established, characterized by velocity oscillations within the range 80–300 m/s, the av-

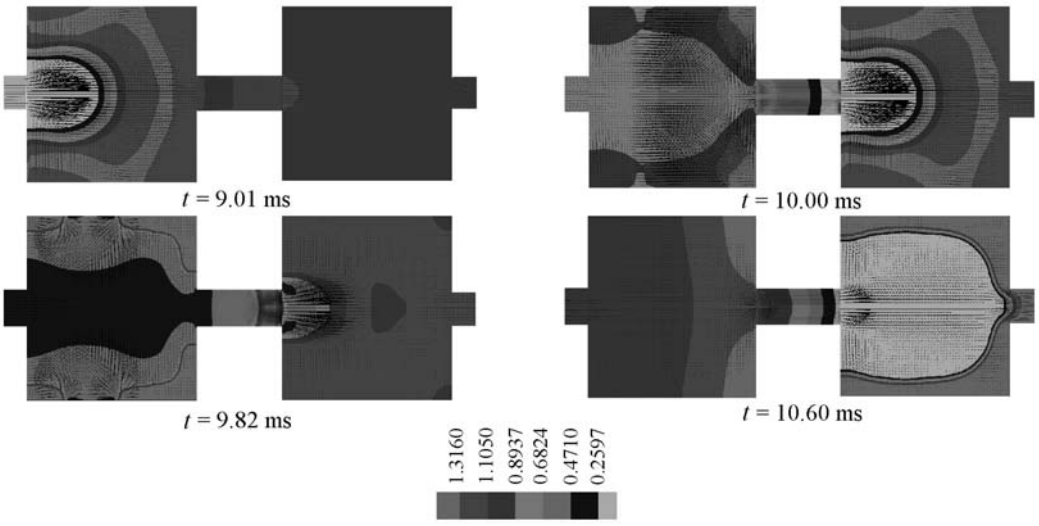

Fig. 12. Density maps in the 6th–7th cavities at $\beta_{ER} = 0.96$ and $C_{fuel} = 0.012$. Mapping colors correspond to different densities (kg/m^3).

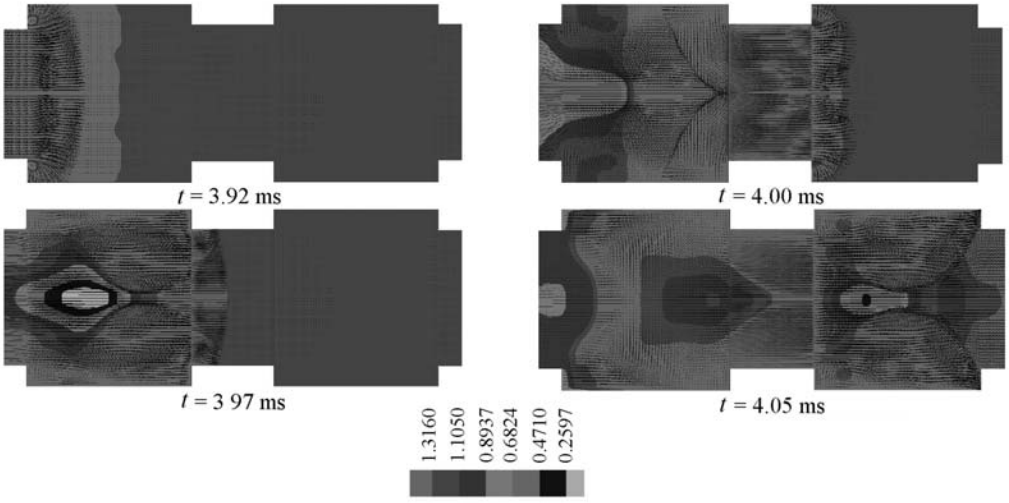

Fig. 13. Density maps in the 6th–7th cavities at $\beta_{ER} = 0.40$ and $C_{fuel} = 0.012$. Mapping colors correspond to different densities (kg/m^3).

erage velocity of the flame front being 156 m/s. The maps of density and velocity for successive times in the section of the tube incorporating cavity numbers 6 and 7 are shown in Fig. 12. It is seen that in each cavity combustion passes through similar stages: flame penetration from the tube, expansion and slowing down in the cavity, being pushed into the next tube, accelerating due to continuing combustion in the cavity. Thus, the process has a periodic character.

The results of numerical experiments show that increasing the number of turbulizing cavities did not promote DDT for the present configuration but just the opposite — it prevented the onset of detonation and brought about the establishing of a galloping combustion mode. The effect took place due to very sharp jumps of the cross-section area in the cavities and periodic slowing down of the flame due to its expansion.

To characterize the cross-section area jumps within the structures of such type, one can use the expansion-ratio parameter and the volume-ratio parameter:

$$\beta_{ER} = \frac{S_{chamb} - S_{tube}}{S_{chamb}}; \quad \alpha_{ER} = \frac{S_{chamb}L_{chamb} + S_{tube}L_{tube}}{S_{chamb}\,(L_{chamb} + L_{tube})} = 1 - \frac{\delta\beta_{ER}}{1+\delta}; \quad \delta = \frac{L_{tube}}{L_{chamb}},$$

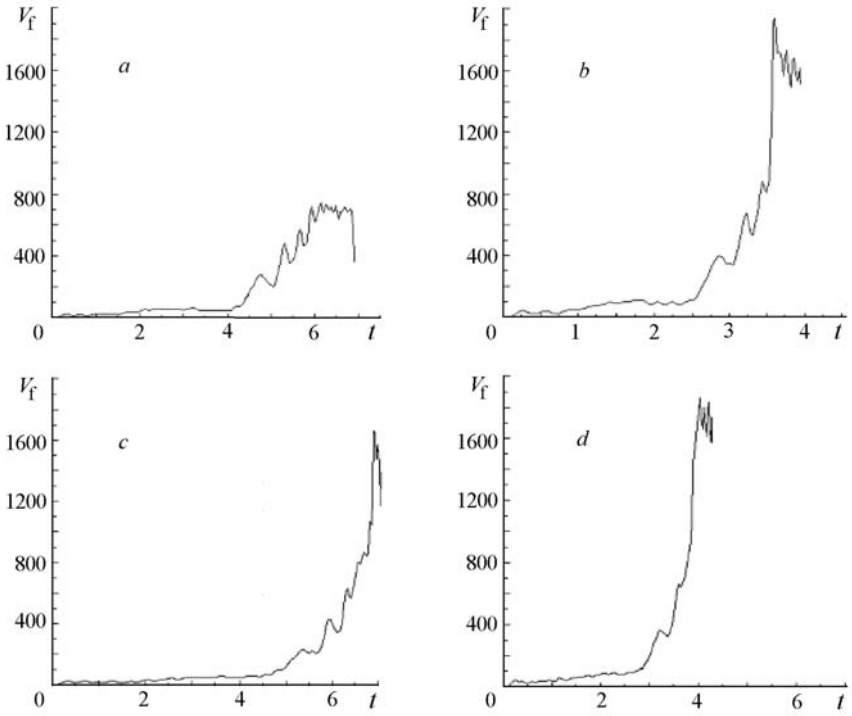

Fig. 14. Reaction-front velocities in a tube with 10 cavities for different fuel concentrations and expansion ratios: a) C_{fuel} = 0.012, β_{ER} = 0.60; b) 0.015, 0.60; c) 0.012, 0.40; d) 0.015, 0.40. V_f, m/s; t, ms.

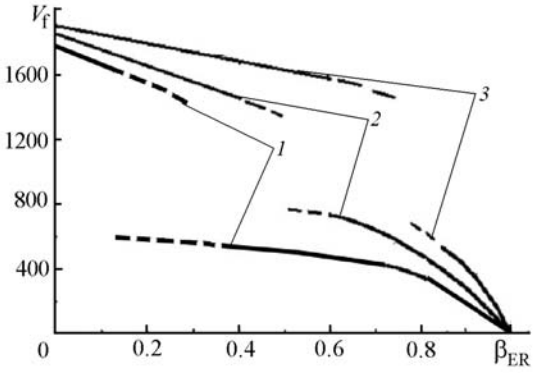

Fig. 15. Mean reaction-front velocity in a multicavity tube versus expansion ratio for different concentrations: 1) C_{fuel} = 0.011; 2) 0.012; 3) 0.015. V_f, m/s.

where S_{chamb} is the cavity cross-section area, S_{tube} is the cross section of the tube, L_{tube} is the length of the bridge connecting the two cavities, L_{chamb} is the length of a cavity of wider cross section. In our experiment, the expansion ratio was very high (β_{ER} = 0.96), which could promote flame acceleration in the beginning of the tube but blocked it in other parts.

To investigate the influence of the expansion ratio on the onset of detonation, a set of numerical experiments was carried out on the DDT in tubes with diameters of 64.3 mm and 76.7 mm that incorporated similar cavities 100 mm in diameter and 100 mm long. These two cases correspond to expansion-ratio parameter values of 0.60 and 0.40, respectively. The tube incorporated 10 cavities distributed uniformly with 50 mm in intervals, the whole structure thus being 1.45 m long.

Figure 13 illustrates gas density and velocity fields in the 6th–7th cavities for successive times when the reaction front was passing through these cavities (expansion ratio β_{ER} = 0.40). Fuel volume concentration (C_{fuel} = 0.012) and ignition conditions were the same as in the previous case (Fig. 12). The results of numerical modeling show that

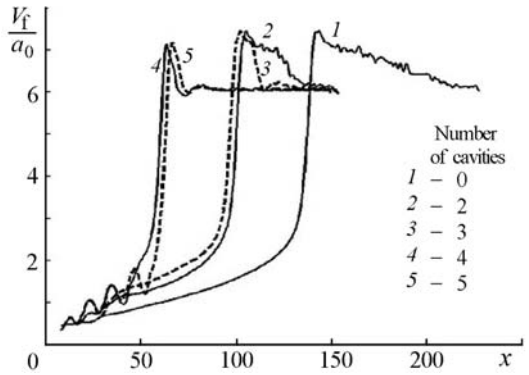

Fig. 16. Reaction-front velocity variation in DDT for different number of cavities incorporated into the ignition section of the device: 1) without cavities; 2) two cavities; 3) three cavities; 4) four cavities; 5) five cavities. *x*, mm.

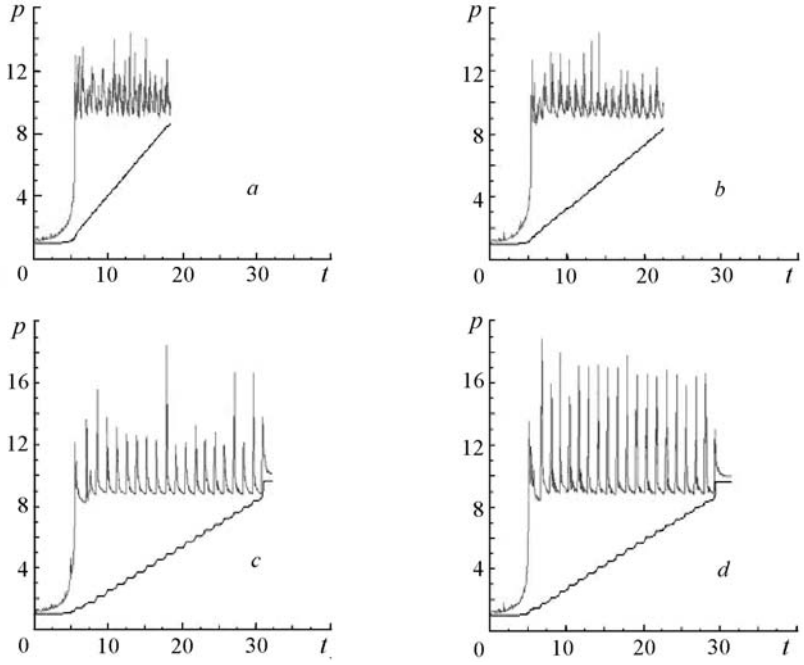

Fig. 17. Pressure in the combustion device versus time at different values of the volume ratio α_{ER}: oscillating curves correspond to maximal pressure, continuous curve — to the average pressure in the whole device; a) α_{ER} = 0.808; b) 0.68; c) 0.52; d) 0.36. *p*, bar; *t*, ms.

the onset of detonation took place between the 7th and 8th cavities. The maximal velocity of an overdriven detonation was 1700 m/s, average velocity 1450 m/s. Thus, in the present case we can talk about low-velocity detonation having been established within the tube.

Figures 14a and c and 18 illustrate flame-front velocities for combustion propagation in a tube incorporating uniformly distributed cavities of wider cross sections for one and the same fuel concentration, 0.012. It is seen from the figure that for high values of the expansion ratio low-velocity galloping combustion was established with very regular velocity oscillations (Fig. 18). For lower expansion ratios, high-velocity galloping combustion characterized by irregular oscillations of much smaller amplitude was established. For even smaller expansion ratios, low-velocity galloping detonation was established, characterized by an average velocity much less than that of Chapman–Jouguet for the given mixture composition.

Thus, for the mixture composition considered, the expansion ratios between 0.40 and 0.60 are transient ones, wherein changing of the flame-propagation regime from high-speed galloping combustion to low-velocity galloping

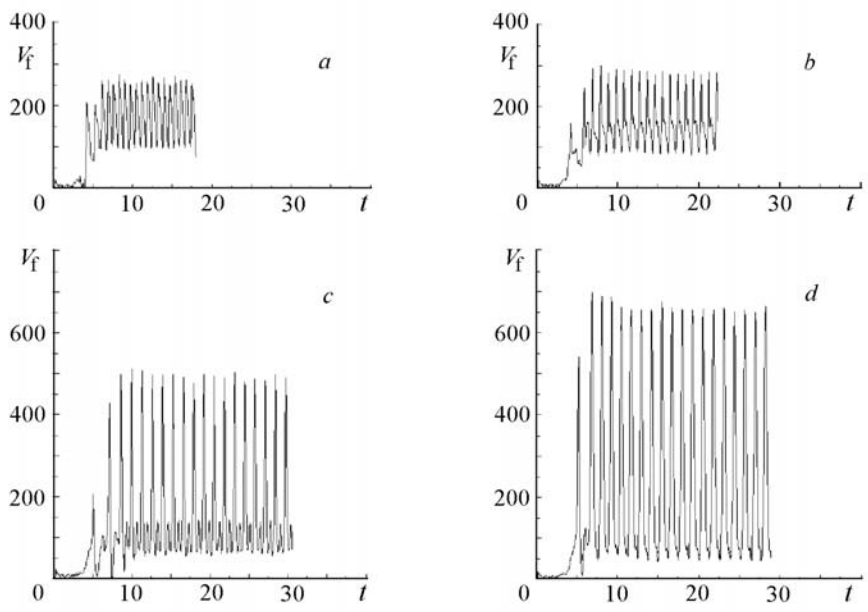

Fig. 18. Combustion-front velocity versus time for different values of α_{ER}: a) 0.808; b) 0.68; c) 0.52; d) 0.36. V_f, m/s; t, ms.

detonation takes place. Let us investigate the influence of the mixture composition on transient values for the expansion ratio. Figure 14a and b illustrates the results of numerical experiments on flame acceleration in a multicavity tube for different values of the initial fuel concentration (C_{fuel} = 0.012 and C_{fuel} = 0.015) but for one and the same value of the expansion ratio (β_{ER} = 0.60). Figure 14c and d shows flame trajectories and mean axial velocities for the same fuel contents, but for a different value of the expansion-ratio parameter (β_{ER} = 0.40).

Figure 14a and b shows that for the fuel concentration C_{fuel} = 0.012 and expansion ratio β_{ER} = 0.60 high-velocity galloping combustion was established in the tube propagating at an average velocity of 720 m/s. For the higher fuel concentration 0.015 and the same expansion ratio, the accelerating galloping combustion regime changed in the 6th cavity to a low-velocity galloping detonation, which was propagating at an average speed of 1600 m/s with a maximal speed of 2000 m/s in the transition zone. Thus, an increase in the initial fuel concentration brings about an increase for transient values of the expansion-ratio parameter β_{ER}.

Figure 14c and d shows reaction-front mean velocities in a similar tube with 10 cavities for another expansion ratio (β_{ER} = 0.40) but the same values of fuel concentrations (C_{fuel} = 0.012 and C_{fuel} = 0.015). It is seen that for both mixture compositions DDT takes place for the present moderate value of the expansion ratio. But the increase in fuel concentration from 0.012 up to 0.015 shortened the predetonation length (transition took place in the 5th cavity instead of the 8th) and increased the mean value of the galloping detonation velocity from 1450 m/s up to 1650 m/s.

Figure 15 shows the velocities of self-sustained modes of reaction-zone propagation in tubes incorporating cavities of wider cross sections uniformly distributed along the axis as functions of expansion ratio and fuel concentration. It is seen that the transient values of the expansion ratios increase with increase in the fuel concentration.

Evaluating the effect of turbulizing cavities of wider cross section incorporated into a detonation tube on the DDT process, it should be noted that the presence of fore-cavities in the ignition section of the tube promotes flame acceleration and stabilizes DDT. On the other hand, the established detonation wave could degenerate on entering a cavity of large expansion ratio, which brings about the suppression of detonation. What is the optimal number of cavities to be integrated into the ignition section that could promote DDT? Numerical modeling undertaken for the expansion ratio β_{ER} = 0.96 shows that two cavities were enough for the adopted values of governing parameters.

A theoretical explanation for the effect is based on the necessary condition for the DDT to be satisfied — the Zeldovich criterion for the so-called coupling of gas dynamics processes (compression-wave generation ahead of the flame) and chemical physics and transport phenomena, which govern the flame-front propagation [20, 24, 48, 49]. This criterion actually means that the flame-propagation velocity should exceed the speed of sound in the unburned gas mixture. Analysis of results (Fig. 16) shows that the piston effect of expanding reaction products in fore-cavities brings

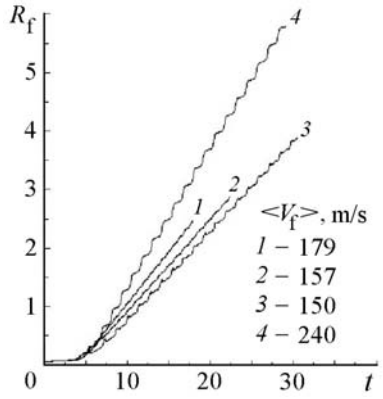

Fig. 19. Front position versus time in a tube incorporating cavities at β_{ER} = 0.96 for different values of α_{ER}: 1) α_{ER} = 0.808; 2) 0.68; 3) 0.52; 4) 0.36. R_f, m; t, m/s.

about a rapid acceleration of the flame on entering a narrow tube. On leaving the first cavity and entering the narrow tube between the two cavities, flame accelerates up to velocities of 110–260 m/s, depending on the fuel concentration (Fig. 16), which turns out to be less than the sonic velocity. On leaving the second cavity, the flame is pushed into the detonation tube at a speed of 435–920 m/s, which already surpasses the necessary criterion. Thus, further increase in the number of cavities is no longer necessary.

Under different values of governing parameters (expansion ratio, mixture composition, and temperature, etc.) the necessary number of cavities can be different. Let us consider as an example flame acceleration and DDT in a tube with cavities incorporated so that the expansion ratio β_{ER} = 0.75 and volume ratio α_{ER} = 0.78; ignition conditions and mixture composition will be kept constant (hydrogen–oxygen mixture, 30% dilution of nitrogen). It is seen from the figure that increasing the number of cavities promotes DDT but consumes the time for flame propagation inside the cavities. For the present conditions, four cavities give the optimal number, and further increase in this number increases predetonation length.

The Influence of Volume Ratio on the Onset of Detonation in Tubes with Cavities. To investigate the volume-ratio-parameter effect on the combustion-wave propagation modes and onset of detonation, numerical simulations were performed for different distances between the cavities, while the diameter of the tube and diameter of the cavities were constant. That provided a constant value for the expansion-ratio parameter, thus allowing volume-ratio-parameter variation only. The usual parameters were: cavity radius 5 cm; bridge radius 1 cm; cavity length 10 cm; expansion ratio 0.96.

The following four cases were considered: *a*) bridge length 2.5 cm; $\alpha_{ER} = 0.808$; 20 cavities, length 10·20 + 2.5·19 = 247.5 cm; bridge/cavity length ratio 2.5/10 = 0.25; *b*) bridge length 5 cm; $\alpha_{ER} = 0.68$; 20 cavities, length 10·20 + 5·19 = 295 cm; bridge/cavity length ratio 5/10 = 0.5; *c*) bridge length 10 cm; $\alpha_{ER} = 0.52$; 20 cavities, length 10·20 + 10·19 = 390 cm; bridge/cavity length ratio 10/10 = 1.0; *d*) bridge length 20 cm; $\alpha_{ER} = 0.36$; 20 cavities, length 10·20 + 20·19 = 580 cm; bridge/cavity length ratio 20/10 = 2.0.

Figure 17 illustrates pressure oscillations and average pressure in the device for the four different volume ratios. It is seen in the figure that a decrease in volume ratio brings about an increase in pressure oscillation amplitude.

Figure 18 illustrates flame-velocity variation for the same four cases. Comparison of results shows that a decrease in volume-ratio parameter causes an increase in the velocity oscillation amplitude: maximal velocity increases and minimal velocity decreases with volume-ratio decrease.

Figure 19 illustrates flame trajectories for the cases considered. The results show that the dependence of the mean flame velocity on volume-ratio parameter is not monotonic. In the considered interval, a velocity minimum for a volume ratio of 0.52 is observed.

Numerical simulations performed for different values of the expansion ratio showed that for an expansion ratio of 0.60 a decrease in volume ratio from 0.80 down to 0.60 brings about an increase in flame-front velocity, while volume-ratio variation in the interval 0.88–0.80 does not bring about substantial changes in flame velocity, which could indicate the vicinity of velocity minimum. For an expansion ratio of 0.40, a decrease in volume ratio from 0.92 down

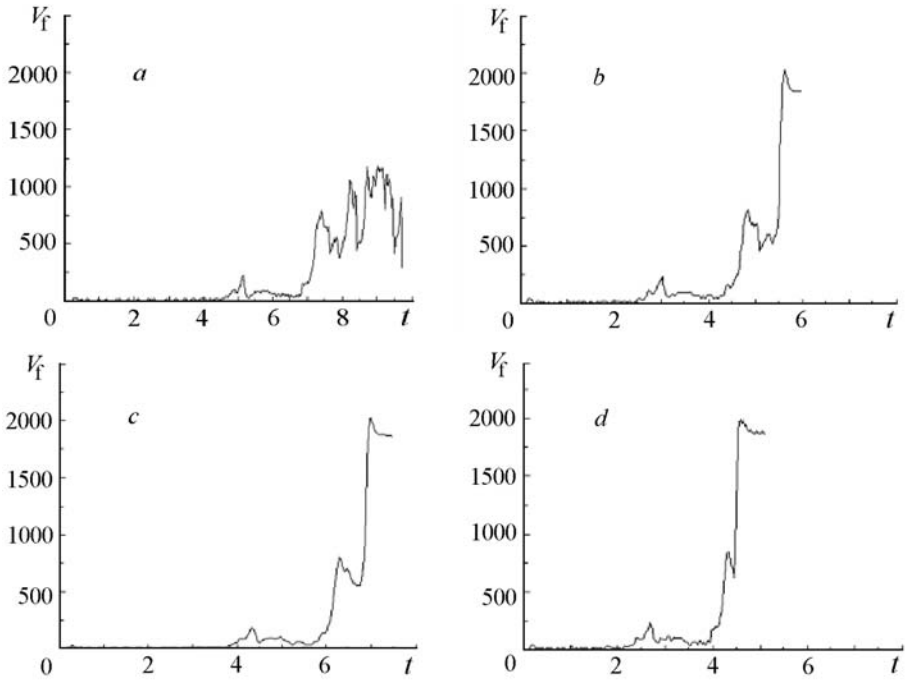

Fig. 20. Flame-zone cross-section averaged axial velocity in a two-cavity tube at β_{ER} = 0.96 and C_{fuel} = 0.011 (a and b) and 0.012 (c and d) for normal [a and c) T_0 = 300 K] and elevated [b and d) T_0 = 353 K] temperatures. V_f, m/s; t, ms.

to 0.73 does not bring about any substantial variation in mean flame-front velocity and in the amplitude of oscillations, which could be explained by the fact that the onset of detonation takes place for the present expansion ratio for all volume ratios.

Investigation of the combustion front in a tube with two cavities in the ignition section for an expansion ratio of 0.96 and different length ratios of the two cavities showed that an increase in the length ratio until a definite value promotes DDT in gases. Further increase in the length ratio of cavities increases the predetonation time and length.

The Influence of Initial Gas Temperature on the DDT in Detonation Tubes with Fore-Cavities. The influence of temperature on the DDT in gases is an intriguing issue. The available experimental data on the influence of initial mixture temperature on the DDT process in gases is contradictory. The experiments on DDT in stoichiometric hydrogen–oxygen mixtures in tubes of constant cross section at a constant pressure showed an increase in predetonation length with increase in temperature [46]. On decreasing the content of hydrogen, a substantial influence of initial mixture temperature on the predetonation length was not detected within the temperature range 311–473 K [47]. Investigations of DDT in hydrocarbon fuel–air mixtures [17] in tubes incorporating fore-cavities in the ignition section demonstrated a decrease in predetonation length with increase in the initial mixture temperature.

The reason for the results being contradictory lies deep in the physical chemistry of the phenomenon, wherein the increase in initial mixture temperature gives birth to two opposite effects. On the one hand, the increase in temperature promotes chemical reactions, thus promoting flame acceleration due to kinetic reasons. On the other hand, transition to detonation takes place after the relative velocity of turbulent flame propagation surpasses the speed of sound in the gas, which increases with temperature increase, thus inhibiting the transition process. The decrease in density on increasing the temperature at a constant pressure could also be considered an inhibiting factor. It is probably due to the competition of these opposite effects that the available data on the influence of initial mixture temperature on the DDT process in gases is contradictory.

As has already been mentioned, in stoichiometric hydrogen–oxygen mixtures an increase in temperature brought about an increase in predetonation length [46]. Those results indicate that for hydrogen–oxygen mixtures in tubes of constant cross section the effect of sound-velocity increase with increase in temperature is predominant as compared with the effect of flame-speed increase. Thus, the combination of both effects retards the DDT.

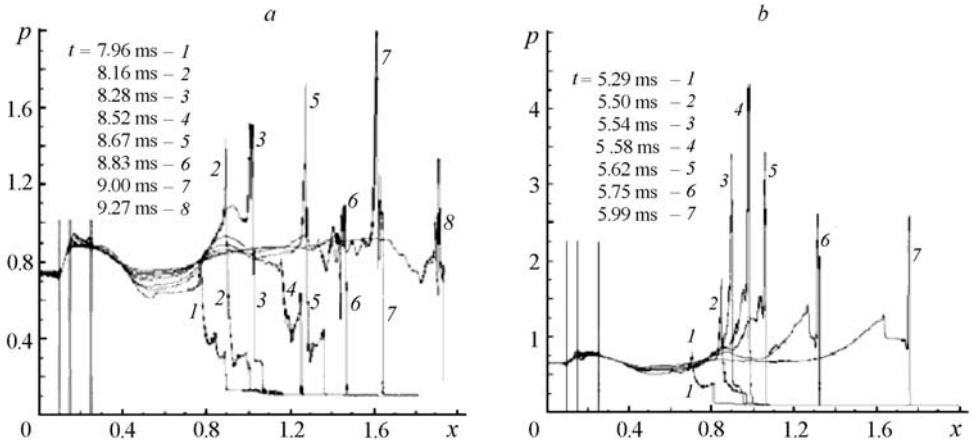

Fig. 21. Successive pressure profiles for combustion propagation in tubes incorporating two cavities in the ignition section for normal [a) T_0 = 300 K] and elevated [b) T_0 = 353 K] temperatures. p, MPa; x, m.

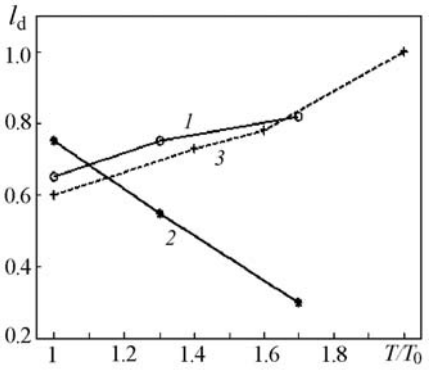

Fig. 22. Predetonation length as a function of initial temperature for a hydrogen–air stoichiometric mixture: 1) tube of constant diameter; 2) tube incorporating four cavities in the ignition section; 3) experiments in a smooth tube [75, 76]. l_d, m.

In our investigations of the DDT in tubes incorporating cavities of wider cross section [17, 19, 28], we rely heavily on the role of a piston effect of the expanding reaction products, which penetrate the narrow tube from a wide cavity, thus pushing the turbulent flame in the tube, assisting it in achieving high velocities surpassing the velocities of sound. Results of numerical modeling (Fig. 9) show that on leaving the second cavity the flame being pushed into the narrow tube has a velocity substantially surpassing the sonic velocity, which is due to gas-dynamics effects. Thus, the decrease or increase in sonic velocity in the initial mixture due to temperature variation could hardly influence the criterion to be satisfied. The use of turbulizing fore-cavities neutralizes the negative effect on DDT of sound-velocity increase with increase in temperature. Thus, the effect of reduction of chemical induction time with increase in temperature could turn out to be predominant.

Numerical simulations of ignition and flame propagation in lean mixtures (fuel concentration C_{fuel} = 0.011–0.012) at an elevated initial temperature showed that an increase in the initial temperature of the combustible mixture brings about shortening of the predetonation length and time. Figure 20 shows the flame velocities in a two-cavity tube for two values of the fuel concentration (C_{fuel} = 0.011 and 0.012) for normal (T_0 = 300 K) and elevated (T_0 = 353K) temperatures. Figure 21 illustrates successive pressure profiles for combustion propagation in tubes incorporating two cavities in the ignition section for two different temperatures. As is seen, the onset of detonation takes place only at an elevated temperature.

It is seen from Fig. 20a and b that at C_{fuel} = 0.011 in the case of low temperature (T_0 = 300 K) the onset of detonation did not take place within the length of the test section. High-speed galloping combustion occurred for

that low fuel concentration. For higher temperature (T_0 = 353K), DDT took place and a stable detonation mode was achieved via an overdriven regime (Fig. 21b).

On increasing the fuel concentration (C_{fuel} = 0.012), the DDT takes place for both temperatures (Fig. 22c and d). Nevertheless, the onset of detonation in the case of elevated temperature takes place earlier than for the lower temperature. It is also seen that an increase in temperature in the present numerical experiment brought about a decrease in the predetonation length.

Figure 22 illustrates the dependence of predetonation length on initial temperature for a hydrogen–air stoichiometric mixture for a tube of constant diameter [56] and a tube incorporating four cavities [57] in the ignition section. Simulations were performed for small ignition energy and a tube diameter of 40 mm and cavity diameter of 80 mm. For comparison, a dashed line is provided in Fig. 22, which illustrates results of experiments [75, 76] in a smooth tube.

In summarizing, it should be noted that in detonation tubes with wider fore-cavities in the ignition section an increase in the initial mixture temperature promotes DDT and shortens the predetonation length, while in tubes of constant cross section (without any fore-cavities) the effect of initial temperature increase could be the opposite. Thus, the role of mixture temperature in detonation initiation can be discussed only in conjunction with the role of geometrical factors.

CONCLUSIONS

The experimental and theoretical investigations show that the onset of a detonation wave in the DDT process takes place in local exothermic centers ("hot spots") between the accelerating zone of turbulent combustion and the leading shock wave. Those hot spots appear due to flow nonuniformity, mostly on the contact discontinuities formed due to the interaction of flame and shock waves overtaking each other ahead of the flame zone.

Depending on the internal structure of the hot spots they could give birth to either deflagration or detonation waves. In the case of detonation onset, the detonation wave propagates in all directions from the source and finally forms a detonation wave propagating ahead and a retonation wave propagating backward. The detonation wave overtakes the leading shock, and after their interaction a quasi-plane overdriven detonation wave is formed in the unburned mixture, which gradually slows down to a self-sustained Chapman–Jouguet mode.

In the case where the hot spot gives birth to a deflagration wave, its propagation in all directions from the exothermic center is much slower, which allows enough time for other hot spots to reach autoignition and in the long run could bring about the onset of detonation.

The presence of several cavities of wider cross section in the ignition zone shortens the pre-detonation length for hydrocarbon–air gaseous mixtures and makes the onset of detonation more stable.

An increase in the number of similar cavities uniformly distributed along the tube could block the onset of detonation and lead to the establishing of galloping high-speed combustion modes for large expansion ratios or low-velocity galloping detonations for small expansion ratios. The mean reaction-front axial velocity grows with increase in the hydrocarbon fuel concentration in the range 0.010–0.015. For expansion ratios within the range 0.4–0.6, the increase in fuel content could bring about a change in the propagation regime: a galloping combustion mode could be changed to a low-velocity detonation regime. Transient values of the expansion ratio, which characterize the transition from low-velocity detonation to a high-speed galloping combustion, increase with increase in the fuel concentration within detonability limits.

Increasing the number of turbulizing cavities in the ignition section promotes DDT until the flame velocity on leaving the last cavity surpasses the sonic velocity. Further increase in the number of cavities inhibits DDT.

For large expansion ratios (0.96), a decrease in the volume-ratio parameter causes an increase in the velocity oscillation amplitude and maximal pressure oscillation amplitude. The dependence of the mean flame velocity on the volume-ratio parameter is not monotonic. In the considered interval, a velocity minimum for a volume ratio of 0.52 is observed.

For a smaller expansion ratio (0.60), a decrease in the volume ratio from 0.80 down to 0.60 brings about an increase in flame-front velocity, while the volume-ratio variation in the interval 0.88–0.80 does not bring about substantial changes in flame velocity, which could indicate the vicinity of velocity minimum.

For an expansion ratio of 0.40, the onset of galloping detonation takes place sooner or later for all values of the volume ratio. Increasing the volume ratio increases predetonation time.

A increase in the initial mixture temperature in tubes incorporating fore-cavities of greater diameter in the ignition section promotes DDT and shortens the predetonation length, while in tubes without fore-cavities the effect of temperature increase on DDT could be quite the opposite, bringing about an increase in the predetonation length.

The Russian Foundation for Basic Research (grant 08-03-00190) is acknowledged for financial support.

NOTATION

A_r, Arrhenius factor for the rth reaction depending on temperature T; $\mathbf{a} \otimes \mathbf{b}$, tensor with components $a_i b_j$; C_μ, $C_{1\varepsilon}$, $C_{2\varepsilon}$, C_g, *k-epsilon* model constants; C_{fuel}, fuel volume concentration in the mixture; c_{pk}, c_{vk}, specific heat capacity of the kth gas component at constant pressure and volume, respectively, J/(kg·K); D, overall laminar diffusion coefficient, m^2/s; D_θ, dissipation term for mean-squared temperature deviate, $kg \cdot K^2/(m^3 \cdot s)$; E, specific energy of fluid, J/kg; E_A, activation energy, J; f_μ, f_1, f_2, positive functions ($0 < f_\mu \le 1, f_1 \ge 1, 0 \le f_2 \le 1$) which depend on two local Reynolds numbers; g, mass force vector, m/s^2; h_{0k}, specific internal energy of the kth gas component, J/kg; $\mathbf{I}_k$, turbulent diffusive flux of the kth component, $kg/(m^2 \cdot s)$; $\mathbf{I}_q$, turbulent energy flux, $J/(m^2 \cdot s)$; $\mathbf{J}_q$, turbulent conductive heat flux, $J/(m^2 \cdot s)$; K_j, pre-exponential factor; k, turbulent kinematic energy, J/kg; L, length of the detonation tube, m; L_b, length of a bridge, m; L_c, length of a chamber, m; L_{chamb}, length of a cavity of a wider cross section, m; L_{tube}, length of a bridge connecting the two cavities; l_d, predetonation length, m; N, number of components within the gas phase; $\mathbf{n}$, normal vector to a wall; P_d, probability density function; P_θ, production due to the chemistry term for the mean-squared temperature deviate, $(kg \cdot K^2)/(m^3 \cdot s)$; p, pressure, Pa; R, radius of the cylindrical vessel, m; R_f, reaction flame position, m; R_t, R_y, local Reynolds numbers; $R_g = 8.31$, universal gas constant, J/(mol·K); r, radial coordinate in Descartes' coordinate system, m; S_{chamb}, cavity cross-section area, m^2; S_{tube}, cross section of the tube, m^2; T, temperature of the gas, K; T_0, initial temperature, K; T_{aj}, activation temperature, K; T_{mj} — minimum temperature, K; t, time, s; t_0, time of ignition, s; $\mathbf{U}$, unit tensor of the 2nd range; $\mathbf{u}$ — fluid velocity vector, m/s; V, velocity of the leading disturbance, m/s; V_f, front velocity, m/s; W_k, molar mass of the kth gas component, kg/mol; W_θ, production due to the chemistry term for the mean-squared temperature deviate, $kg \cdot K^2/(m^3 \cdot s)$; x, axial coordinate in Descartes' coordinate system, m; Y_k, mass fraction of the kth gas component; α_{ER}, volume-ratio parameter; β_{ER}, expansion-ratio parameter; ε, turbulent energy decay, W/kg; $\theta = \overline{T'T'}$, mean-squared deviate for temperature; θ_m, limiting value for the mean-squared temperature deviate; λ, effective laminar thermal conductivity, $W/(m^2 \cdot K)$; μ, effective laminar viscosity, Pa·s; ν, molecular kinematic viscosity, m^2/s; ν^t, turbulent kinematic viscosity, m^2/s; ρ, gas density, kg/m^3; σ, share of water in hydrocarbon thermal decomposition; $\sigma_d, \sigma_t, \sigma_\varepsilon$, *k-epsilon* model constants; τ, turbulent viscosity tensor, $kg/(m \cdot s^2)$; τ^t, Reynolds tensor term within effective viscosity tensor, $kg/(m \cdot s^2)$; τ^T, transposed tensor τ; $\tau : \theta$, double product of the 2nd range tensors; ϕ, ratio of actual fuel concentration in the mixture to a stoichiometric one; ω_{ij}, specific mass production rate of the ith component via chemical transformations in the jth reaction, $kg/(m^3 \cdot s)$; $\dot{\omega}_k$, specific mass production rate of the kth component via chemical reactions in the gas phase, $kg/(m^3 \cdot s)$; $\nabla \cdot \mathbf{a}$, divergence of the vector $\mathbf{a}$; $\nabla \cdot \tau$, divergence of the tensor τ; ∇p, gradient of the scalar p; $\nabla \mathbf{a}$, tensor with components $\nabla_i a_j$; ∂_t, partial derivative with respect to time.

REFERENCES

1. E. Mallard and H. L. Le Chatelier, Sur la vitesse de propagation de l'inflammation dans les melanges explosifs, *Compt. Rend. Acad. Sci. Paris*, **93**, 145–148 (1881).
2. M. Berthélot and P.Vieille, Sur la vitesse de propagation des phenomenes explosifs dans le gaz, *Compt. Rend. Acad. Sci. Paris*, **93**, 18 (1881).
3. V. A. Mikhelson, On normal combustion velocity of explosive gaseous mixtures, *Uch. Zap. Imper. Moscow Univer., Otd. Phiz. Mat.*, Issue 10, 1–92 (1893).
4. W. J. M. Rankine, On the thermodynamic theory of waves of finite longitudinal disturbance, *Phil. Trans. Roy. Soc. London*, 277–288 (1870).

5. H. Hugoniot, Propagation des mouvements dans les corps et spécialement dans les gaz parfaits, *Journ. Liouville*, **3**, 477–492 (1887); **4**, 153–167 (1888).
6. D. L. Chapman, On the role of explosion in gases, *Phil. Mag*., **47**, 90 (1899).
7. E. Jouguet, On the propagation of chemical reactions in gases, *J. Mathematics*, **1**, 347 (1905).
8. E. Bishimov, V. P. Korobeinikov, V. A. Levin, and G. G. Cherny, One-dimensional unsteady state flows of combustible mixtures accounting for finite rates of chemical reactions, *Fluid Dynamics*, No. 6, 7–19 (1968).
9. V. A. Levin and V. V. Markov, Onset of detonation in concentrated energy input, *Combustion, Explosion and Shock Waves*, **11**, No. 4, 623–629 (1975).
10. V. A. Levin, V. V. Markov, and S. F. Osinkin, Direct initiation of detonation in hydrogen–oxygen mixtures diluted by nitrogen, *Fluid Dynamics*, No. 6, 151 (1992).
11. A. K. Hayashi, H. Shimada, Y. Kenmoku, and H. Sato, Detailed mechanism of flame jet ignition in pulse detonation engines, in: G. Roy, S. Frolov, and J. Shepherd (eds.), *Application of Detonation to Propulsion*, Torus Press Ltd., Moscow (2004), pp. 207–211.
12. G. D. Salamandra, On interaction of a flame with a shock wave, in: *Physical Gas Dynamics*, USSR Acad. Sci. Publ. (1959), pp. 163–167.
13. T. V. Bazhenova and R. I. Soloukhin, Gas ignition behind the shock wave, in: *Proc. 7th Int. Symposium on Combustion*, Buttterworths, London (1959), p. 866.
14. A. K. Oppenheim and P. A. Urtiew, Experimental observations of the transition to detonation in an explosive gas, *Proc. Roy. Soc*., **A295**, 13 (1966).
15. R. I. Soloukhin, *Methods of Measure and Main Results of Experiments in Shock Tubes*, Novosibirsk State University Publ., Novosibirsk (1969).
16. A. K. Oppenheim and R. I. Soloukhin, *Ann. Rev. Fluid Mech*., **5**, 31 (1973).
17. N. N. Smirnov and A. P. Boichenko, Deflagration to detonation transition in gasoline-air mixtures, *Combustion, Explosion and Shock Waves*, **22**, No. 2, 65–68 (1986).
18. R. P. Lindstedt and H. J. Michels, Deflagration to detonation transition in mixtures of alkane LNG/LPG constituents with O_2/N_2, *Combustion and Flame*, **72**, No. 1, 63–72 (1988).
19. N. N. Smirnov and M. V. Tyurnikov, Experimental investigation of deflagration to detonation transition in hydrocarbon-air gaseous mixtures, *Combustion and Flame*, **100**, 661–668 (1995).
20. Ya. B. Zeldovich, V. B. Librovich, G. M. Makhviladze, and G. I. Sivashinsky, On the onset of detonation in a non-uniformly pre-heated gas, *J. Appl. Mech. Techn. Phys. (USSR)*, **2**, 76 (1970).
21. A. G. Merzhanov, On critical conditions for thermal explosion of a hot spot, *Combustion and Flame*, **10**, 341–348 (1966).
22. A. A. Borisov, On the origin of exothermic centers in gaseous mixtures, *Acta Astronautica*, **1**, 909–920 (1974).
23. K. Kailasanath and E. S. Oran, Ignition of flamelets behind incident shock waves and the transition to detonation, *Combustion Science Technology*, **34**, 345–362 (1983).
24. Ya. B. Zeldovich, B. E. Gelfand, S. A. Tsyganov, S. M. Frolov, and A. N. Polenov, Concentration and temperature non-uniformities of combustible mixture as a reason of pressure waves generation, in: A. Kuhl et al. (eds.), *Dynamics of Explosions*, AIAA Inc., New York, **114** (1988), p. 99.
25. N. N. Smirnov, An. Yu. Demyanov, and I. I. Panfilov, Deflagration to detonation transition, *Chemical Physics of Comb. and Expl. Detonation*, USSR Acad. Sci. Publ., 52–56 (1989).
26. P. Wolanski, *Archivum Combustions*, Nos. 3–4, 143–149 (1991).
27. N. N. Smirnov and I. I. Panfilov, Deflagration to detonation transition in combustible gas mixtures, *Combustion and Flame*, **101**, 91–100 (1995).
28. N. N. Smirnov, V. F. Nikitin, A. P. Boichenko, M. V. Tyurnikov, and V. V. Baskakov, Deflagration to detonation transition in gases and its application to pulse detonation devices, in: G. D. Roy et al. (eds.), *Gaseous and Heterogeneous Detonations: Science to Applications*, ENAS Publ., Moscow (1999), pp. 65–94.
29. N. N. Smirnov and V. F. Nikitin, *Comb. Exp. Shock Wave*, **40**, No. 2, 186–199 (2004).
30. Yu. A. Gostintsev, A. G. Istratov, N. I. Kidin, and V. E. Fortov, Self-turbulization of gaseous flames. Theoretical models, *Teplofiz. Vys. Temp.*, **37**, No. 4, 633–637 (1999).

31. Yu. A. Gostintsev, A. G. Istratov, N. I. Kidin, and V. E. Fortov, Self-turbulization of gaseous flames. Experimental data analysis, *Teplofiz. Vys. Temp*, **37**, No. 2, 306–312 (1999).
32. C. J. Brown and G. O. Thomas, Experimental studies of shock-induced ignition and transition to detonation in ethylene and propane mixtures, *Combustion and Flame*, **117**, 861–870 (1999).
33. A. M. Khohlov and E. S. Oran, Numerical simulation of detonation initiation in a flame brush: the role of hot spots, *Combustion and Flame*, **119**, 400–416 (1999).
34. K. I. Shchelkin and Ya. K. Troshin, *Gas Dynamics of Combustion*, USSR Acad. Sci. Publ., Moscow (1963).
35. R. Knystautas, J. H. S. Lee, J. E. Shepherd, and A. Teodorczyk, Flame acceleration and transition to detonation in benzene-air mixtures, *Combustion and Flame*, **115**, 424–436 (1998).
36. M. Fischer, E. Pantow, and T. Kratzel, Propagation, decay and re-ignition of detonations in technical structures, in: G. D. Roy et al. (eds.), *Gaseous and Heterogeneous Detonations: Science to Applications*, ENAS Publ., Moscow (1999), pp. 197–212.
37. N. N. Smirnov and V. F. Nikitin, The influence of confinement geometry on deflagration to detonation transition in gases. *J. Phys. IV France*, **12**, No. 7, 341–351 (2002).
38. R. H. Abdullin, V. S. Babkin, A. V. Borisenko, and P. K. Senachin, *Combustion of Gas in a Linear System of Connected Vessels*, Preprint of Altay Teknn. Univ., Barnaul (1997).
39. N. N. Smirnov, V. F. Nikitin, M. V. Tyurnikov, A. P. Boichenko, J. C. Legros, and V. M. Shevtsova, Control of detonation onset in combustible gases, in: G. D. Roy et al. (eds.), *High Speed Deflagration and Detonation*, Elex-KM Publ., Moscow (2001), pp. 3–30.
40. V. V. Azatyan, The role of chain branching mechanism in ignition and combustion of hydrogen-oxygen mixtures near the third limit, *Kinetics and Catalysis*, **37**, No. 4, 512–520 (1996).
41. M. Philip, *Experimentelle und Theoretische Untersuchungen zum Stabilitatsverhalten von Drallflammen mit zentraler Ruckstromzone*, Dissertation, Karlsruhe University (1991).
42. O. Pironneau and B. Mohammadi, *Analysis of the K-Epsilon Turbulence Model*, Masson Editeur, Paris (1994).
43. E. S. Oran and J. P. Boris, *Numerical Simulation of Reactive Flow*, Elsevier, New York (1987).
44. N. N. Smirnov and V. F. Nikitin, Unsteady-state turbulent diffusive combustion in confined volumes, *Combustion and Flame*, **111**, 222–256 (1997).
45. D. A. Anderson, J. C. Tannehill, and R. H. Pletcher, *Computational Fluid Mechanics and Heat Transfer*, Hemisphere Publ. Co. (1984).
46. P. Laffitte, Influence of temperature on the formation of explosive waves, *Comp. Rendu*, **186**, 951 (1928).
47. L. E. Bollinger, M. C. Fong, and R. Edse, Experimental measurement and theoretical analysis of detonation induction distance, *ARSJ*, **31**, 588 (1961).
48. R. K. Cheng and J. M. Short, Diagnostics of the exothermic process, *Prog. Astronaut. Aeron.*, AIAA Inc., New York, **53**, 611 (1977).
49. J. W Dold and M. Short, Compressibility corrections to Zeldovich's spontaneous flame and the onset of an explosion in a non-uniformly pre-heated medium, in: *Proc. 13th ICDERS*, Nagoya (1991), p. 63.
50. V. P. Karpov, G. G. Politenkova, and E. S. Severin, Turbulent burning of alcohol. *Combustion, Explosion and Shock waves*, **22**, No. 4, 12–14 (1986).
51. N. M. Marinov, A detailed chemical kinetic model for high temperature ethanol oxidation, *Int. J. Chemical Kinetics*, **31**, 183–220 (1999).
52. R. W. Hamming, *Numerical Methods for Scientists and Engineers,* Second Ed., Dover, New York (1986).
53. W. H. Press, S. A. Teukolsky, W. T. Vetterling, and B. P. Flannery, *Numerical Recipes in C: The Art of Scientific Computing*, Second Ed., Cambridge University Press (1992).
54. E. Schultz, E. Wintenberger, and J. Shepherd, Investigation of deflagration to detonation transition for application to pulse detonation engine ignition systems, in: *Proc. 16th JANNAF Propulsion Meeting* (1999).
55. E. S. Oran and V. N. Gamezo, Origins of the deflagration to detonation transition in gas-phase combustion, *Combustion and Flame*, **148**, 4–47 (2007).
56. N. N. Smirnov, V. F. Nikitin, and S. Alyari Shurekhdeli, Transitional regimes of wave propagation in metastable systems, *Combustion, Explosion and Shock Waves*, **44**, No. 5, 517–528 (2008).

57. N. N. Smirnov, V. F. Nikitin, and S. Alyari Shurekhdeli, Investigation of self-sustaining waves in metastable systems: deflagration-to-detonation transition, *J. Propulsion and Power*, **25**, No. 3, 593–608 (2009).
58. N. N. Smirnov and E. I. Shemyakin, Combustion to explosion transformation in metastable media, in: *Modern Problems of Mathematics and Mechanics*, MSU Publ., Moscow (2009), Vol. 1, pp. 245–275.
59. V. F. Nikitin, V. R. Dushin, Y. G. Phylippov, and J. C. Legros, Pulse detonation engines: Technical approaches, *Acta Astronautica*, **64**, 281–287 (2009).
60. V. F. Nikitin, N. N. Smirnov, Yu. G. Phylippov, and E. I. Shemyakin, Detonation onset in transmission from a ring gap into a chamber, *Moscow Univ. Mech. Bull.*, Allerton Press, No. 3, 67–72 (2009).
61. M. A. Liberman, M. Kuznetsov, I. Matsukov, and A. Ivanov, Restructuring of a flame due to a preheated zone as a mechanism underlying the deflagration-to-detonation transition, in: *Proc. 22nd ICDERS*, No. 3, Minsk (2009).
62. M. A. Liberman, M. Kuznetsov, I. Matsukov, and A. Ivanov, Formation of the preheated zone ahead of a propagating flame and the mechanism underlying the deflagration-to-detonation transition, *Physics Letters*, **A 373**, 501–510 (2009).
63. G. H. Markstein, *Nonsteady Flame Propagation,* Macmillan, New York (1964).
64. T. V. Bazhenova and V. V. Golub, Utilization of gaseous detonation in a controlled high frequency regime (review), *Combustion, Explosion and Shock Waves*, **39**, No. 4, 3–21 (2003).
65. D. I. Baklanov, S. V. Golovastov, L. G. Gvozdeva, A. Kaltayev, N. B. Scherbak, and V.V. Volodin, Investigation of transition of deflagration to detonation in moving mixtures of combustible gases, in: *CD Proc. 20th Int. Coll. on Dynamics of Explosions and Reactive Systems*, Montreal, Canada, 31 July–5 August (2005).
66. D. I. Baklanov, L. G. Gvozdeva, and N. B. Scherbak, Pulsed detonation combustion chamber for PDE, in: G. D. Roy et al. (eds.), *High-Speed Deflagration and Detonation: Fundamentals and Control*, ELEX-KM Publishers, Moscow (2001), pp. 239–250.
67. D. I. Baklanov, S. V. Golovastov, V. V. Golub, and V. V. Volodin, Detonation formation in moving detonable mixture flow, in: *Application of Detonation to Propulsion*, G. D. Roy et al. (eds.), Torus Press Ltd., Moscow (2004), pp. 225–231.
68. O. V. Achasov and O. G. Penyazkov, Some gasdynamic methods for control of detonation initiation and propagation, in: G. D. Roy et al. (eds.), *High-Speed Deflagration and Detonation: Fundamentals and Control*, ELEX-KM Publishers, Moscow (2001), pp. 31–44.
69. F. Schauer, J. Stutrud, R. Bradley, V. Katta, and J. Hoke, Detonation studies and performance results for a research pulse detonation engine, in: *Application of Detonation to Propulsion*, G. D. Roy et al. (eds.), Torus Press Ltd., Moscow (2004), pp. 287–302.
70. J. F. Clarke, D. R Kassoy, and N. Riley, On direct initiation of a plane detonation wave, *Proceedings of the Royal Society of London*, **A408**, 129–148 (1986).
71. D. R. Kassoy, J. A. Kuehn, M. W. Nabity, and J. F. Clarke, Detonation initiation on the microsecond time scale DDTs, in: *Collection of Technical Papers — 44th AIAA Aerospace Sciences Meeting 15* (2006), pp. 11453–11512.
72. A. Kaltajev, J. Leblanc, and T. Fujiwara, Influence of turbulence on the deflagration to detonation transition in a tube, in: *Proc. 17th Int. Coll. on the Dynamics of Explosions and Reactive Systems*, Heidelberg, Germany, 31 July–5 August, 1999.
73. K. O. Sabdenov, *Thermo-Physical Hydro-Gas-Dynamical Effects in Combustion of Gases and Rocket Propellants*, Doctoral Dissertation, Tomsk State University, Tomsk (2007).
74. A. M. Starik and N. S. Titova., Initiation of detonation in a supersonic flow behind a shock wave under nonequilibrium excitation of vibrational degrees of freedom of molecules, in: G. D. Roy et al. (eds.), *Gaseous and Heterogeneous Detonations*, ENAS Publ., Moscow (1999), pp. 225–240.
75. D. Powell, P. J. Van Tiggelen, H. Vasatko, and H. G. Wagner, Initiation of detonation in various gas mixtures, *Combustion and Flame*, **15**, 173–177 (1970).
76. A. K. Oppenheim and R. A. Stern, On the development of gaseous detonation. Analysis of wave phenomena, in: *Proc. 7th Int. Symposium on Combustion*, Buttterworths, London (1959), pp. 837–850.
77. G. D. Salamandra, T. V. Bazhenova, and I. M. Naboko, *Zh. Tekh. Fiz.*, **29**, Issue 11, 1354 (1959).